

This item is the archived peer-reviewed author-version of:

Catalyst design by NH_4OH treatment of USY zeolite

Reference:

Van Aelst Joost, Verboekend Danny, Philippaerts An, Nuttens Nicolas, Kurttepel Mert, Gobechiya Elena, Haouas Mohamed, Sree Sreeprasanth P., Denayer Joeri F. M., Martens Johan A.,- Catalyst design by NH_4OH treatment of USY zeolite
Advanced functional materials - ISSN 1616-301X - 25:46(2015), p. 7130-7144
Full text (Publisher's DOI): <https://doi.org/10.1002/ADFM.201502772>
To cite this reference: <https://hdl.handle.net/10067/1302140151162165141>

Hierarchical zeolites are class of superior catalysts which couple the intrinsic zeolitic properties to enhanced accessibility and intracrystalline mass transport to and from the active sites. The on-purpose design of hierarchical USY catalysts is achieved, using a sustainable post-synthetic room temperature treatment with mildly alkaline NH_4OH (0.02 M) solutions. Functionally-relevant implications of the treatment are elucidated by a thorough characterization assessing a broad variety of physico-chemical properties. In addition to routinely-applied techniques, advanced and state-of-the-art high-resolution microscopy and a novel Ar adsorption technique are applied, providing more insight into the connectivity and accessibility of the mesopores. Starting with a commercial dealuminated USY zeolite (Si/Al = 47), a hierarchical material is obtained by selective and tuneable creation of interconnected and accessible small mesopores (2 to 6 nm). In addition, the treatment yields immediately the NH_4^+ form without the need for additional ion exchange. After the NH_4OH modification, the original crystal morphology is retained, whereas micropores content and relative crystallinity are decreased, leading to an increase of the meso-/micropore balance. The gradual formation of dense amorphous phases throughout the crystal without significant framework atom leaching rationalizes the very high material yields (> 90 %). This hierarchization-by-densification concept distinguishes the NH_4OH treatment from other known hierarchization strategies. The superior catalytic performance of the developed hierarchical zeolites is proven by the acid-catalyzed isomerization of α -pinene and the metal-catalyzed conjugation of safflower oil. Significant improvements in activity and selectivity are attained, as well as a lowered susceptibility to deactivation. The catalytic performance can be intimately related to the introduced mesopores, hence enhanced mass transport capacity, and the retained intrinsic zeolitic properties.

1. Introduction

Porous materials are of primary importance in a wide range of applications as catalysts, catalyst supports and adsorbents.^[1,2] Among them, crystalline zeolites comprise an important class owing to their ordered micropores of molecular dimensions (0.25–1 nm, ultra-micropores), resulting in large specific surface areas and allowing shape-selective catalysis. Moreover, they exhibit specific acid properties and excellent ion exchange capacity for various guest cations. Compared to other porous materials, zeolites usually show high hydrothermal stability, whereas textural and acidic properties can be easily controlled or modified.^[1,2] As a result of the unique features, zeolites are widely used not only in petrochemical industries^[3,4] as catalysts and catalyst supports, but also in traditional ion-exchange, adsorption and separation applications.^[1,4,5] Also in emerging bio refinery processes zeolites are gradually becoming more widely applied.^[6,7,8] Furthermore, zeolites have potential in emerging applications for electronics, optical and sensor technologies.^[2,9]

Despite the unique shape selective properties, restricted utilization of the intracrystalline zeolite voids in catalysis is often faced due to slow diffusion of molecules to and from the active sites located in the micropores.^[10] Today, treatment of heavy crude oil-derived feedstocks^[11] and renewable feeds, like vegetable oil and (ligno)cellulose, necessitates optimization of the zeolite accessibility to such bulky substrates.^[8,12] Whereas novel zeolites have been proposed with larger pore sizes^[13] or reduced crystal size^[14], their industrial potential is hampered due to costly synthesis procedures and practical issues such as poor filtration behavior or low stability.^[10,15] Zeolites with hierarchical pore architecture – *i.e.* zeolite crystals containing simultaneously interconnected mesopores and micropores –

suitably solve this site-accessibility problem.^[2,10,16] The zeolitic micropores bear the catalytic function, while the additionally created larger pores ensure access of larger molecules and enhanced intracrystalline mass transport.

Different synthesis procedures using templating and non-templating techniques have been developed to synthesize hierarchically structured zeolites.^[10,17] Alkaline treatment (desilication) creates intracrystalline mesopores by hydrolysis of framework (Si and/or Al) atoms and seems industrially most viable.^[15,18] Importantly, processing parameters such as alkali source and concentration of solution, temperature and contact time, should be carefully tuned in order to obtain genuine hierarchical zeolites with interconnected micropores and mesopores, the latter being accessible directly from the external surface of the crystals. Moreover, the synthesis process parameters heavily depend on the specific requirements of the application, and consequently on the nature of the zeolite framework and its composition, especially the Si/Al ratio.^[19]

Formation of mesopores in zeolites by alkaline treatment usually occurs by aqueous NaOH treatment. It has already been studied in detail for many zeolite topologies such as MFI, MOR and BEA.^[19,20,21] Recently, this technique was also applied to create mesopores in USY zeolites.^[22-24] It was pointed out, however, that siliceous 12-membered ring zeolites, such as highly dealuminated USY, are extremely sensitive to these alkaline treatments, resulting in amorphization and considerable loss of material. To obtain hierarchical zeolites with preserved intrinsic zeolitic properties, Verboekend *et al.* optimized the base leaching procedure for USY zeolites by adding organic pore-directing agents such as tetrapropylammonium cations (TPA⁺). Although effective, the method involves dissolution of copious amounts of solid (35 – 50 wt%).^[15,23,24] Moreover, the use of organic pore-directing agents or organic bases preferably should be avoided in order to realize a sustainable and economically attractive manufacture of hierarchical zeolites. Very recently, efforts were made

to largely recover the used organic compounds, using the volatile diethylamine as an organic leaching agent.^[15]

After alkaline treatments with NaOH, ion-exchange steps are necessary to obtain the NH₄-form of the zeolite. The latter is needed not only for easy and complete ion exchange with counter cations and metal ion salts, but also to obtain an acid catalyst after calcination. For this reason, aqueous NH₄OH has been studied as an alternative base for the base leaching of MFI zeolites.^[25] However, the attempts appeared unsuccessful, attributed to the weak alkalinity of NH₄OH. Matsuura *et al.* also applied a NH₄OH treatment on H-ZSM-5 zeolites, resulting in the formation of an additional acid site type, the pore architecture of the zeolite being fully retained.^[26] Furthermore, a mesostructured zeolite USY was successfully synthesized with NH₄OH.^[27] However, cetyltrimethyl ammonium (CTA⁺) addition as a structure-directing agent was necessary, which needs to be removed by combustion. Later, it was suggested that these mesostructured materials are best described as zeolite/OMM composites.^[28]

Recently, we treated commercially available and highly dealuminated USY zeolites with highly diluted NH₄OH solutions at room temperature in absence of any protecting or structure-directing agent.^[29] An XRD and MAS NMR study has been performed on these materials, revealing the partial and gradual formation of amorphous phases containing silanol nests, strongly bound ammonium and highly structured water molecules in close interaction with each other.^[30] In this study, an advanced and thorough characterization, including state of the art Ar adsorption and high-resolution microscopy, results in an analysis of functionally relevant physico-chemical implications of the NH₄OH treatment. Special attention is paid on the material yield, introducing a novel mesopore formation mechanism based on a partial and controllable densification. Furthermore, the potential of the resulting hierarchical zeolites is demonstrated in two different catalytic conversions of bulky biomass-derived substrates,

thereby establishing links between the material structure/properties and its catalytic function. The acid properties of the material are utilized for the isomerization of a terpene molecule, *viz.* α -pinene.^[7,31-33] Its role as effective support for highly dispersed noble metals, *viz.* Ru, is demonstrated for the conjugation of safflower oil, *viz.* a highly unsaturated vegetable oil rich in linoleic acid.^[34,35]

Results and Discussion

A commercially available, severely steamed and acid-leached H-USY zeolite (H-USY(40)) is subjected to mild (0.02 M) NH₄OH treatments at room temperature for varying treatment times, followed by calcination (**Table 1**). First, the influence on porosity and morphology is studied (Section 2.1), including visualization of the formed mesopores and assessment of the pore connectivity and accessibility. Furthermore, structural properties and acidity are examined (Section 2.2). The material yield, elemental composition and implications on the pore formation mechanism are discussed in Section 2.3. Finally, the catalytic significance of the applied post-synthetic treatment is proven for two conversions of bulky biomass-derived molecules (Section 2.4).

2.1 Porosity and morphology

The influence of the NH₄OH treatment on the pore-architecture is monitored by Ar physisorption (at 87 K) and applying the Density Functional Theory (DFT) method on the obtained isotherms. This technique enables analysing accurately surface area, average pore size, pore size distribution and porosity over the complete micropore/mesopore size range, avoiding the potential problems of strong interaction associated with N₂ isotherms.^[36-38] The parent H-USY(40) sample already contains substantial intracrystalline mesoporosity (0.27 cm³ g⁻¹), due to steaming and acid leaching treatments, as evidenced by the hysteresis

phenomenon apparent in the type IV isotherm (**Figure 1 (a)**). The additional NH_4OH treatment clearly affects the shape of the isotherm in the low-pressure range ($p/p_0 < 0.4-0.5$), significantly decreasing the specific volume of the original zeolite Y micropores ($p/p_0 < 0.01$), while generating larger pores leading to the increased Ar adsorption at higher relative pressures ($0.01 < p/p_0 < 0.4-0.5$). The derived pore size distributions, obtained by the NLDFT model,^[37] reveal that the newly formed pores are very uniform small mesopores, centered around 4 nm (**Figure 1 (b)**). Furthermore, it is apparent that the large mesopores, around 10-30 nm, already present in the parent H-USY(40) zeolite, are not affected by the NH_4OH treatment (**Figure S1**). In our previous study on the same materials, the BJH method applied on the N_2 adsorption isotherm, resulted in a pore width of 2-3 nm for the formed mesopores.^[30] Procedures based on a modified Kelvin equation, such as BJH, are known to underestimate in certain cases the pore size for pores smaller than 10 nm.^[38] Noticeably, USY zeolites with trimodal pore architecture, *viz.* micropores (1.2 nm, Y zeolite structure), small mesopores (s-meso of 2-6 nm, mainly generated by NH_4OH treatment) and large mesopores (6–30 nm, steam treatment/acid leaching), are present after contacting a highly dealuminated USY zeolite with a diluted NH_4OH solution.

The quantification of the respective specific pore volumes and surface areas via the NLDFT method^[37] is summarized in Table 1. Clearly, a considerable amount of small mesopores (2-6 nm), *viz.* $0.22 \text{ cm}^3 \text{ g}^{-1}$, is already formed after contacting the USY zeolite for 0.25 h with a 0.02 M NH_4OH solution, while the specific volume of micropores (V_{micro} ; < 2 nm) decreases from 0.27 to $0.16 \text{ cm}^3 \text{ g}^{-1}$. The total specific mesoporous volume (V_{meso}) and surface (S_{meso}) eventually increases, respectively from 0.27 to $0.40 \text{ cm}^3 \text{ g}^{-1}$ and from $181 \text{ m}^2 \text{ g}^{-1}$ to $311 \text{ m}^2 \text{ g}^{-1}$. The simultaneous decrease of V_{micro} with the increase of S_{meso} (**Figure 2 (a)**) results in an equally large indexed hierarchy factor,^[21] calculated by a multiplication of a relative mesoporosity ($V_{\text{meso}}/V_{\text{meso,max}}$) by a relative microporosity ($V_{\text{micro}}/V_{\text{micro,max}}$), *i.e.* $IHF =$

$(V_{micro}/V_{micro,max})*(S_{meso}/S_{meso,max})$ (Figure 2 (b)). Nevertheless, the NH_4OH treatment is expected to result in a decreased susceptibility to diffusion limitations, as a major increase of the V_{meso}/V_{micro} ratio is observed (Figure 2 (b)). The latter can be correlated to the ratio of intracrystalline mass transport capacity to activity in a catalytic transformation. In contrast to reported $NaOH$ base treatments applied on USY zeolites,^[22-24] the original larger mesopores (> 6 nm) remain almost unaltered. For example, when treating H-USY(40) with 0.2 M $NaOH$ at 338 K, the formed mesopores have a larger width of 4 to 12 nm (**Figure S2** (a)). Meanwhile, all micropores disappear upon contact with the 0.2 M $NaOH$ as a result of the harsh treatment conditions. When the zeolite is treated with NH_4OH for longer times, V_{micro} continues to decrease, while V_{s-meso} and V_{meso} increases up to a treatment time of 5 h, the specific surface area values following the same trends (Figure 2 (a)). In contrast to the equal IHF values (≈ 0.5) obtained after short treatments ($\leq 1h$), longer treatments lead to lower IHF values as a result of the relatively strong decrease of V_{micro} . On the other hand, the V_{meso}/V_{micro} value keeps increasing upon treatment time (Figure 2 (b)). The NH_4OH treatment is also effective when a USY zeolite with a lower Si/Al of 30 is treated (**Table S1**). However, it should be noted that USY with Si/Al as low as 15 is not sufficiently susceptible anymore to effective mesopore formation with the proposed mild NH_4OH treatment.

In order to effectively enhance diffusion, the formed mesopores should be interconnected to a maximum degree and easily accessible from the external crystal surface without too many narrow restrictions. Recently, a new method for determining accessibility of mesopores in nanoporous materials was presented.^[39] It allows estimating the fraction of mesopores (< 16 nm) accessible from the external crystal surface without restricted pore mouth, by using the hysteresis in the mesopores during Ar sorption experiments. As in this method the Ar isotherm is also measured at the temperature of liquid nitrogen (77 K) or even lower, i.e. well below the bulk boiling point of Ar (87 K) and its bulk triple point (82.8 K), hysteresis and

consequently pore accessibility can also be measured for smaller mesopores below 4 nm.^[40] At 77 K, Ar will not completely fill pores above 16 nm as pore filling will only occur until the bulk sublimation line is reached.^[40] Mercury porosimetry also gives information on accessibility of pores, but cannot probe small mesopores^[41], present in very significant quantity in the materials studied here. Figure 1 (c) shows the Ar isotherms measured at 87 and 77 K on H-USY-B, respectively probing all pores or only the ones with size below 16 nm, the latter showing a reduced total specific adsorbed volume at comparably high p/p_0 . The larger specific volumes adsorbed at 77 K in the lower p/p_0 range result from the higher density of liquid Ar (1.45 g cm⁻³ at 77 K, against 1.40 g cm⁻³ at 87 K). Note that the actual densities in the pores may be somewhat different, as the density of confined Ar, believed to be supercooled liquid, depends on the pore size.^[37] The desorption branch of both isotherms shows a characteristic step down, at p/p_0 0.45 and 0.35 respectively for 87 and 77 K, caused by cavitation of pores emptying through a restriction. Two important values can be extracted from the 77 K isotherm (Figure 1 (c)), *viz.* the specific volume of mesopores contributing to the step down in the hysteresis loop ($V_{\text{meso,step down}}$) and the total specific volume of pores smaller than 16 nm ($V_{\text{total,<16 nm}}$ with closure point at p/p_0 of about 0.97). Using the Gurvich rule and an estimated value of 1.45 g cm⁻³ for the Ar density, both volumes can be quantified (Table 1). As expected, total specific pore volumes determined at 77 K are lower than at 87 K, as pores larger than 16 nm are not completely filled by condensation at 77 K.^[40] From $V_{\text{total,<16 nm}}$, the specific volume of mesopores smaller than 16 nm ($V_{\text{meso,<16 nm}}$) can be derived by subtraction of V_{micro} (obtained from 87 K isotherm). To assure the isotherm drop is really caused by pores accessible through a smaller restriction, scanning isotherms were recorded for H-USY-B at 77 K. Clearly, all desorption scans starting at different relative pressures after partial pore filling, all return to the desorption boundary curve in the regime of the characteristic step down (Figure 1 (d)). The fraction of restricted mesopores can be

determined only for pores smaller than 16 nm and is given by the ratio of $V_{\text{meso,step down}}$ and $V_{\text{meso,<16 nm}}$. Table 1 shows these values for H-USY(40), H-USY-A, H-USY-B and H-USY-C.

It can be concluded that in all treated samples, at least 65-70 % of the mesopores (< 16 nm) is accessible via the crystal surface without any restriction. This is a lower bound for the total accessible mesopore fraction, as a similar analysis of the 87 K isotherms, now including all pores above 4 nm, results in slightly lower restricted mesopore fractions (not shown). It also follows that the fraction of restricted mesopores for the parent H-USY(40) zeolite is smaller than for the treated samples, increasing from 21 to 30-35 %. This implies that part of the newly formed mesopores is restricted. Similar values obtained by hysteresis analysis for both high-silica USY zeolites and hierarchical variants have been reported earlier.^[39,42] However, in those studies a systematic evaluation of pore accessibility comparing both parent and treated USY zeolites was lacking. Unfortunately, neither the size of the restricted pores nor the size or nature of restrictions can be deduced from the measurements. Restricted mesopores may consist of cavities surrounded by micropores, but they can also still have a good accessibility, only potentially hampered by the presence of a smaller mesoporous entrance. Practically, this means that larger reactant and product molecules might have access to more mesopores than the lower bound of 65-70% estimated above.

Despite the drastic changes in pore architecture upon NH_4OH treatment, no morphologic changes in the zeolite crystals could be visualized by high-resolution SEM (HR-SEM) (**Figure 3**). The particle shape and size are well preserved, even after a treatment time of 16 h. As sample coating is not a prerequisite for HR-SEM, the occurrence of surface pitting is obvious. However, no difference in surface porosity between parent and NH_4OH treated material was shown, as the smallest HR-SEM observable pores have a diameter of approximately 7 nm and the larger mesopores are already present in the steamed parent material. Moreover, also no changes in surface roughness or surface deposits could be

detected. These observations confirm the mildness of the method and contrast the morphology changes after applying a treatment with 0.2 M NaOH at 338 K on H-USY(40). In the latter case severe morphology breakdown and crystal fragmentation clearly occurs (see **Figure S2** (b)).

In order to visualize small scale transformations, electron microscopy measurements including HAADF-STEM electron tomography were performed on samples H-USY(40), H-USY-A and H-USY-D (**Figure 4**). Animated versions of the tomograms are provided in the supporting information as videos. Electron tomography reconstructions show that in addition to micropores, the parent H-USY(40) zeolite mainly contains large mesopores (Figure 4; **Figure S3**). Most importantly, these experiments confirm the increase of the relative abundance of the third pore type by NH₄OH treatment, *viz.* the small mesopores at 2-6 nm. Furthermore, it is obvious from the representative pores in Figure 4 (c, f and i) that the small mesopores are connected among themselves, with other pore types and with the external surface of the zeolite crystal/particle. These results suggest that the main part of the restricted mesopores (as assigned by Ar physisorption) are not cavity-shaped. The restricted Ar desorption is likely to be caused by the presence of a smaller pore entrance. In conclusion, electron tomography confirms the formation of a hierarchical material with interconnection of the three different pore size levels and good accessibility to the external crystal surface.

2.2 Characterization of structure and acidity

To examine ongoing structural changes during the NH₄OH treatment, infra-red spectra of USY zeolite framework vibrations were recorded with FTIR (**Figure 5** (a)) using the KBr-wafer technique. Bands around 650-500 and at 820-750 cm⁻¹ have been assigned to the stretching vibrations of double six-membered rings (D6R) and the symmetrical stretching mode of zeolite TO₄ tetrahedra, respectively.^[43] With respect to the parent USY zeolite, the

intensity of both typical vibration bands is decreased in the shortly NH_4OH treated sample, whereas they are disappeared after a long treatment (16 h), indicative of a transformation towards a less ordered (amorphous) silica-alumina. This trend is confirmed by quantitative XRD analysis (Figure 5 (b)), evidencing a 30 % relative XRD-crystallinity loss after treatment of 0.25 h (**Table 2**), gradually decreasing further upon longer treatments and thereby correlating well with the loss of V_{micro} , only deviating for the longest treatment (**Figure 6 (a)**). After 16 h almost all Bragg peaks characteristic for faujasite topology have disappeared, resulting in a crystallinity loss of 93 %, while a broad amorphous SiO_2 feature, around 20–30 degree 2θ , appears. As a result of the ongoing distortion process, the unit cell gradually contracts with treatment time, as indicated by the shift to the right of the diffraction peaks (Figure 5 (b)). Interestingly, the opposite trend is observed when USY is treated with NaOH ,^[22] confirming the different impact of the proposed NH_4OH treatment.

^{29}Si MAS NMR (**Figure S4 (a)**) indicates the gradual decrease of the $\text{Q}^4_{\text{ordered}}$ Si-species (-107 ppm) upon NH_4OH treatment, whereas the amount of $\text{Q}^4_{\text{disordered}}$ (-112 ppm), and to a lesser extent that of the Q^3 (-101 ppm) and Q^2 Si-species (-91 ppm) increases. These results confirm that the NH_4OH treatment transforms the original USY material into a less ordered structure with a high condensation state (Q^4) - containing silanol groups.^[30] These silanol groups were also characterized by FTIR spectroscopy of the OH-region (**Figure S5**). As H-USY(40) is obtained via severe dealumination, a significant amount of lattice terminating silanol groups is present at 3745 cm^{-1} .^[44] As a result of NH_4OH treatment, the silanol intensity increases and a broader OH band is formed, pointing to the presence of hydrogen bound hydroxyls in an amorphous silica phase.^[45]

The zeolite sample appears to be predominantly amorphous after a long NH_4OH treatment (*e.g.* 16 h for H-USY-D) from an XRD, IR and MAS NMR point of view. High-resolution STEM yields similar indications, monitoring a decrease of crystallinity with increasing

treatment time. However, since TEM is a more local technique than, for instance, XRD, it is possible to observe long treated zeolitic particles still showing lattice fringes and therefore crystallinity. These lattice fringes with interplanar spacing of 0.27 nm are presented in **Figure 7 (f)** from sample H-USY-D. For the parent and shortly treated zeolites, Figure 7 ((b) and (d)) show interplanar spacings of 1.4 and 1.65 nm, respectively corresponding to the (111) and (110) lattice planes in the FAU topology.^[46]

The characteristic tetrahedrally coordinated aluminosilicate framework of zeolites results in Brønsted acid sites. The FTIR spectrum of H-USY(40) (**Figure S5**) shows two different types, namely high frequency (HF) bridged silanol vibrations (BSV) around 3640 cm^{-1} ($\text{O}_1\text{-H}$ in supercages) and low frequency (LF) BSV around 3550 cm^{-1} ($\text{O}_3\text{-H}$ vibrating in 6-ring).^[47] Due to the NH_4OH treatment, the relative intensities of the BSV signals decrease, depicting a loss of Brønsted acidic sites, as confirmed by FTIR-monitored desorption after pyridine saturation (Table 2). As was the case for the relative crystallinity, also the determined Brønsted acid density is correlated well with the obtained V_{micro} values (Figure 6 (b)), confirming the good reliability of these measurements. For the more extensively treated H-USY-D sample also a significant decrease of the strongest acid site fraction, which still chemisorb pyridine at 623 K, is observed. These changes are not surprising as ^{27}Al MAS NMR reveals transformation of the molecular structure of Al species (Figure S4 (b)). The decrease of the Brønsted acid density can be ascribed to a decrease of tetrahedrally coordinated framework Al (63 ppm).^[48,49] The FTIR spectra also reveal the presence of Lewis acid bound pyridine molecules (1455 cm^{-1}) in both the parent and the NH_4OH treated samples. The concentration of the latter species is enhanced as a result of the NH_4OH treatment (**Figure S6**). The increase of Lewis acid sites is most probably related to the formed Al-species at 57 ppm, as all other identified Al-species decrease upon NH_4OH treatment. This Al-species has been attributed to tetrahedrally coordinated non-framework Al or distorted framework Al.^[49,50,51] MQMAS

experiments confirmed its tetrahedral coordination.^[30] The occurrence of distorted tetrahedral aluminum as Lewis acid sites has been proposed earlier in a publication on hydrothermally dealuminated Y zeolites.^[51] Also partial reintegration of leached Al into the zeolitic framework, leading to a broadening of the framework Al MAS NMR signal, was reported to create Lewis acid sites.^[21,52]

2.3 Densification *versus* leaching strategies

Surprisingly, for all samples treated with aqueous NH₄OH solution aluminum extraction was absent and silicon extraction only occurred to a minor extent (5 %), as measured in the filtrates by elemental analysis. Analysis of the Si and Al content of H-USY(40) and H-USY-D samples shows a decreasing bulk molar Si/Al ratio in the same degree of order (2 %), which can be extrapolated to all samples (Table 2). These results are in line with the high and relatively invariable material yields (90-94 wt%; Table 2) obtained for all treatment times, leading to high ‘desilication efficiencies’, amounting to a maximal value of 30 m² g⁻¹ %⁻¹ for H-USY-C.^[21,53] Note that since the pH of the 0.02 M NH₄OH solution is 10.8, close to the solubility limit of silica in water at room temperature,^[54] it can be postulated that upon contacting the USY zeolite with 0.02 M NH₄OH aqueous solution, similar to a classic base leaching method, Si is extracted from the zeolite framework by OH⁻ mediated hydrolysis, resulting in larger pores. However, as OH⁻ ions are being consumed and the pH slightly decreases, the locally extracted silicate species should re-precipitate in or on the zeolite as a denser amorphous phase, as the pH locally becomes too low to keep them soluble. This hypothesis is confirmed by an extensive MAS NMR study performed on this material.^[30] As Ar sorption indicates substantial pore constriction and HR-SEM images are free of surface debris, precipitation likely occurs in the crystal porosity.

To assess the role of the base type used in this process, the parent H-USY(40) zeolite was treated for 0.25 h with a 0.63 mM NaOH solution with the same initial pH of 10.8. The N₂ physisorption isotherm (77 K) on the calcined sample reveals that such treatment hardly shows any effect on the pore architecture of the parent USY(40) zeolite (**Figure S7**), in contrast to the severe structural changes obtained with NH₄OH at the same pH. As NH₄OH is a weak base ($K_b = 1.8 \cdot 10^{-5}$), most NH₄OH should not be dissociated in aqueous solution, whereas NaOH completely dissociates (**Figure 8**). Each time an OH⁻ anion is consumed by hydrolysis, NH₄OH locally dissociates to maintain the equilibrium, resulting in a better local pH control. Consequently, the total amount of theoretically available OH⁻ is much larger than in a NaOH solution with comparable initial pH. The elegant buffering effect is assumed to be at the basis of the observed differences (Figure 8). Possibly, also cationic NH₄⁺ plays a role in the pore formation process, e.g. in stabilizing intermediate anionic species or surfaces. From our earlier reported extended XRD and MAS NMR study,^[30] it follows that ammonium ions associated with distorted zeolite lattice Al, highly structured water and an abundant number of silanol groups in amorphous silica-alumina domains are typical species in NH₄OH treated USY zeolite.

As no significant amounts of Si or Al are leached during mild NH₄OH treatment, it can be concluded that this mild alkaline treatment differs from all other presently applied alkaline treatments to USY (**Figure 9**). The described gradual partial transformation of USY zeolite by NH₄OH into denser amorphous phases yields only small mesopores in absence of significant material leaching and weight loss, without the use of organics (Figure 9 (I;a)). The pH of a traditionally used solution for base leaching is usually significantly higher, *viz.* pH 12.7 – 13.3 for 0.05 – 0.2 M NaOH. In that case, also larger mesopores are created by a combination of amorphization and framework atom leaching to the filtrate, the extent of the latter being dependent on the treatment conditions (Figure 9 (I;b)).^[22,23] In addition, NaOH treatments will

always require an additional NH_4^+ ion exchange when the acid form is needed, while the strong basic character of NaOH makes it more difficult to control the hierarchization process, an efficient quench to cease the treatment process being required. In combination with CTA^+ as organic micelle-forming cationic surfactant, hydrothermal NH_4OH treatment also results in partial amorphization and significant material leaching (20 wt%), while at least a part of the formed small mesopores are ordered (Figure 9 (I;c)).^[28] This process thus produces a material comparable to our hierarchical USY, but additionally requires organics and a hydrothermal step. On the other hand, alkaline treatment of USY with NaOH in the presence of the organic pore directing agent TPA^+ results in mesopore formation by extensive material leaching, while microporosity and crystallinity of the remaining material are not altered (Figure 9 (I;d)). Indeed, when contacting a USY zeolite ($\text{Si}/\text{Al} = 30$) at 338 K with 0.2 M NaOH and 0.2 M TPABr, a material yield of only 56% was obtained in order to create mesopores while retaining the specific micropore volume ($V_{\text{micro}}/\text{g}$).^[23,24] Thus, in general, if the intrinsic zeolite properties are to be preserved completely, the formation of S_{meso} has to be coupled to a complete extraction of dissolved framework atoms from the zeolite. In the case of USY, this is only achievable with copious amounts of organics.

In many catalytic applications, such as fluid catalytic cracking (FCC), the technical catalyst is present in a macroscopic body, comprising, besides USY zeolite crystals, a significant fraction of mesoporous silica-alumina which serve to provide mechanical strength and attrition resistance (Figure 9 (I;e)).^[55,56] Although they generally lack microporosity, these mesoporous materials typically feature substantial mesoporosity. Therefore, a physical mixture of silica-alumina and conventional USY zeolite may give rise to the same bulk porous properties as the NH_4OH -treated samples. For example, assuming a $V_{\text{micro}} = 0$ and $V_{\text{meso}} = 0.75 \text{ cm}^3 \text{ g}^{-1}$ for the silica-alumina,^[7] a physical mixture with weight ratio 1:1 would yield a V_{micro} of $0.14 \text{ cm}^3 \text{ g}^{-1}$ and a V_{meso} of $0.51 \text{ cm}^3 \text{ g}^{-1}$, that is, exceeding the porosities of

samples H-USY-C and H-USY-D. However, the activity of the zeolite is not enhanced by the presence of the silica-alumina, as the accessibility inside the zeolite crystal remains suboptimal. Therefore, especially in reactions that require strong Brønsted acidity, the silica-alumina merely lowers the catalytic performance by diluting the zeolite fraction.

2.4 Catalytic evaluation

The ultimate goal of the hierarchization of zeolites is to attain enhanced performance in conventional and novel catalytic applications. Particularly interesting are new applications of hierarchical zeolites in biomass conversions, as they generally imply rather bulky feedstocks. The catalytic efficiency of the hierarchical zeolites was therefore tested in two biomass related reactions.

α -Pinene isomerization is a relevant reaction for the catalytic evaluation of hierarchical zeolites, as acid sites in a more accessible pore architecture are expected to influence the catalytic activity.^[7,31,57] This renewable feedstock, easily extractable from wood turpentine oil, via acid-catalyzed isomerization leads to various chemicals, serving as building block for various fine chemicals useful in the pharmaceutical and fragrance industry.^[32] The first step in the reaction pathway requires Brønsted acid sites for pinanyl cation formation, which subsequently can rearrange into monocyclic or bicyclic isomerization products, respectively via limonene and camphene as the primary products.^[7,58] Monocycles are considered as intermediates in the consecutive formation of coke compounds via polymerization.^[59]

The parent and all NH₄OH treated USY zeolites were tested as a catalyst for this conversion, to provide insights into the relation between their structure, properties and function. Dependent on the NH₄OH treatment time, conversion *vs.* reaction time plots (**Figure 10** (a)) show different behaviours with respect to the parent zeolite, indicating higher activities for shortly treated zeolites (H-USY-A and H-USY-B) and lower activities for H-USY-C and H-

USY-D. In Figure 10 (b), the initial activity ($\text{g g}^{-1} \text{hr}^{-1}$) of all studied catalysts is plotted against the NH_4OH treatment time. In comparison with the parent zeolite, a short treatment of 0.25 h leads to an enhancement of the initial activity by a factor of 2.2. Since the treated sample displays an external surface 1.7 times that of the parent, the enhanced activity also implies that the treatment makes the external surface more functional. The latter is attributed to the fact that the secondary porosity in conventional USY zeolites is derived from steaming and/or acid leaching.^[4] The resulting mesopores are not necessarily connected^[41] and do not always contribute to enhancement of the catalytic activity.^[19] The enhanced performance of sample H-USY-A yields concomitantly an increase of the turnover frequency (TOF; on total Brønsted acid basis) by a factor of 3.8 to $5 \text{ mol mol}^{-1} \text{ s}^{-1}$, thereby overcompensating the lowered amount of active sites available. As previously discussed in Figure 2 (b), the parent and the 0.25 h NH_4OH treated USY have an almost equal IHF. Therefore, as two distinctly different materials can display the same IHF, a higher IHF is not a prerequisite to obtain a more active catalyst. Longer NH_4OH treatments gradually result in lower initial activities, although relatively to the parent still resulting in an improvement after 1h treatment. This gradual decrease can be attributed to a dominant effect of the reducing amount of active sites. In contrast the controlled formation of intracrystalline amorphous silica species in USY zeolites by NH_4OH -treatment, the addition of extracrystalline amorphous silica-alumina would lead to a totally different performance. Since amorphous silica-alumina display a substantially inferior catalytic performance compared to that of H-USY(40) (**Table S2**), a physical mixture (*vide supra*, Figure 9 (I;e)), should only lower the catalytic performance. Apart from the activity, also the selectivity of a catalyst is crucial to evaluate its performance. The selectivity towards all mono- and bicyclic products is not influenced by the NH_4OH treatment (Figure 10 (c)). Nevertheless, the underlying product distribution changes. The longer the USY zeolites are treated with NH_4OH , the higher the selectivity for the primary formed isomerization products (camphene and limonene), at the expense of the secondary

products. This effect can be rationalized by the increased balance of intracrystalline mass transport capacity to activity, leading to a lower susceptibility to secondary reactions, which is confirmed by the correlation with the V_{meso}/V_{micro} ratio (Figure 10 (d)). Related to this, TGA analysis after washing and drying of the used catalysts indicates that H-USY(40) contains 20 wt% of coke at 78 % conversion, whereas H-USY-A only contains 12 wt% at complete conversion. These results imply that the NH_4OH treated catalyst has a lower tendency towards cokes formation, which can be ascribed to the faster desorption and diffusion of coke precursors out of the zeolite. This typical characteristic for performant hierarchical zeolites could result in an improved catalyst stability and lifetime.^[60] Furthermore, a thermal regeneration of the recuperated H-USY-A under oxygen atmosphere is carried out, followed by re-use in the isomerization reaction. A quasi-identical performance was observed (Table S3), assuring the intrinsically stability of the hierarchical catalyst under both the reaction and regeneration conditions.

The heterogeneous conjugation of safflower oil is used as second reaction, evaluating the effectiveness of hierarchical zeolites as support for noble metals, *viz.* ruthenium. Safflower oil contains a high amount of linoleic acid, a polyunsaturated C18:2 (*cis*-9, *cis*-12) fatty acid, present as glycerol ester (Figure 11 (a)). The two double bonds of linoleic acid can be catalytically conjugated to different positional and geometrical isomers, forming conjugated linoleic acid (CLA).^[29,34,35] These compounds are of high interest since they are important food and feed additives,^[61] and they find industrial application as coating composition in paint, varnish, glue and inks.^[62] Most known health effects are ascribed to the kinetically favored primary *cis*-9, *trans*-11 and *trans*-10, *cis*-12 isomers, while for industrial applications all CLA isomers are useful, amongst them the more thermodynamically stable secondary *trans*, *trans* CLA isomers. Possible unwanted products during the isomerization reaction are non-conjugated C18:2 isomers and hydrogenated products. The noble metal Ru is loaded on both a

pristine USY(40) and a NH_4OH treated zeolite, viz. USY-C. The more basic sodium exchanged form of both supports was used, which has been proven to have a beneficial effect on the selectivity in the conjugation of linoleic acid.^[35] At first instance, the corresponding ethyl esters of safflower oil are used as reactant, experiencing no beneficial effect of the NH_4OH treatment on the linoleate conversion rate (Figure 11 (b)). On the other hand, when converting the more bulky triglyceride molecules in safflower oil, the linoleate conversion rate is effectively increased (Figure 11 (c)), suggesting a major alleviation of diffusion limitation. Eventually, this results in a higher total CLA yield and productivity. (Figure 11 (d)). Furthermore, the selectivity towards the primary, thermodynamically less favorable CLA isomers is improved as well, as indicated in Figure 11 (d). This can be attributed to a shorter overall residence time of intermediately formed products on the active sites and accordingly to a lower tendency to undergo secondary reactions, like subsequent isomerization to the thermodynamically more favorable *trans,trans* isomers in the consecutive reaction scheme.

2. Conclusion

Mass transport issues in catalytic conversions of bulky substrates necessitate the search for more accessible hierarchical zeolite catalysts, preferably obtained in a cost-efficient way. The interaction of a highly dealuminated USY zeolite with a diluted aqueous NH_4OH solution at room temperature is a straightforward, efficient, and easy-tuneable method to develop highly performant hierarchical zeolite catalysts. Extended and advanced characterization shows major transformations in the porosity, structure and acidity of the USY zeolite upon NH_4OH treatment. An interconnected and well accessible network of small mesopores (2-6 nm) is created, at the expense of the zeolitic micropores. Meanwhile, crystal morphology and size are perfectly retained in absence of significant leaching of Si and Al species. The latter is explained by the gradual formation of intracrystalline dense amorphous phases at the buffering conditions of NH_4OH , inducing a decrease of degree of ordering in the material.

The mild and controllable character of the method enables to tune the degree of mesopore formation and zeolite preservation. The presented method obviously differs from established alkaline treatments, considering the obtained high material yield, the absence of organics used, the retained crystal morphology and the narrow size distribution of the newly formed small mesopores. Moreover, the resulting NH_4^+ counter cation enables the direct transformation of the material into its acid or metal complex loaded form, without applying additional ion exchange steps. The excellent behavior in the isomerization of α -pinene and conjugation of safflower oil clearly illustrates the superior functionality of these new zeolite-based hierarchical materials in the catalytic conversion of (lipid) biomass, both for acid and metal-catalyzed reactions.

3. Experimental Section

Material synthesis

The parent material used in this study is a CBV780 USY zeolite (*Zeolyst International*, bulk Si/Al = 47, H-form), denoted as H-USY(40). The H-USY(40) sample (2.5 g) is added to a alkaline NH_4OH solution (0.02 M, 200 $\text{cm}^3 \text{g}^{-1}$) and stirred at 250 rpm for various treatment times (Table 1). Subsequently, the solution is filtered and washed (3x) with distilled water using a Büchner set-up. The remaining solid is dried overnight at 373 K, weighed and compared to the 373 K dried equivalent of the starting material. To obtain the protonic form of the zeolites, the samples are calcined in a flow reactor under nitrogen ($2 \text{ cm}^3 \text{ s}^{-1} \text{ g}^{-1}$). First, the sample is heated to 473 K (2 K min^{-1} ; 30 min at 473 K) and then the temperature is raised to 623 K (3 K min^{-1} ; 30 min at 623 K). In order to ensure a homogeneous gas flow through the sample, the zeolite powder was pelletized, crushed, and sieved. The 250 – 500 μm pellets were retained for further use. To study the influence of the parent Si/Al ratio, also USY zeolites CBV760 and CBV720 from *Zeolyst International*, are treated with NH_4OH in the

same manner as described above. In the same way, a treatment with aqueous NaOH was performed. In this case, a H-USY(40) sample (2.5 g) is added to an aqueous NaOH solution (pH 10.8; 200 cm³ g⁻¹) and stirred at 250 rpm for 15 minutes. The pH of the solution was determined using a calibrated *Mettler Toledo* Seven Compact S220 pH meter. Subsequently, the solution is filtered and washed (3x) with distilled water using a büchner set-up. The resulting solid is dried overnight at 373 K. After pelletizing, the samples are treated in a flow reactor following the same temperature program as for the calcination procedure (*vide supra*).

When performing the NaOH treatment described by Verboekend *et al.*^[23] on H-USY(40), the zeolite (6.6 g) is added to a NaOH solution (200 cm³, 0.2 M) and vigorously stirred for 30 min at 338 K. The solution is quenched, filtered and washed with distilled water. The resulting powder is dried for 36 h at 338 K. Then, sample pellets are treated in a flow reactor following the temperature program used for the calcination procedure (*vide supra*).

Alternatively, to obtain the NH₄-form of the zeolite without NH₄OH treatment and associated porosity changes, the parent H-USY zeolite was contacted with NH₃ gas in a flow reactor, according to the following procedure: (1) to remove residual water, heating under flowing N₂ at 5 K min⁻¹ to 573 K and remaining there for 3 h; (2) cooling down to 323 K under flowing N₂; (3) contact for 15 min at 323 K with flowing NH₃; (4) heating under flowing N₂ at 5 K min⁻¹ to 473 K and remaining there for 3 h. The obtained NH₄-zeolites, either via gaseous NH₃ or NH₄OH treatment, were transformed in the Na-form via two successive room temperature ion-exchange steps (16 h) with 200 cm³ of an aqueous 1 M NaCl solution per g of dry zeolite. After each exchange step, the slurry is filtered, the solids washed three times with distilled water and air dried at 373 K.

The (NH₄-/Na)USY supports were loaded with 0.5 wt% Ru by ion exchange for 24 h under stirring of the aqueous zeolite slurry, containing the required amount of Ru precursor (Ru(III)(NH₃)₆Cl₃) in 200 cm³ water per gram of dry zeolite. Afterwards, the Ru-hexamine

exchanged zeolite powder was filtered, washed with distilled water and dried overnight at 323 K. Prior to activation the dry powders are compressed, crushed and sieved. The 250 – 500 μm fraction was retained for further use. Activation was conducted in a flow reactor in two steps under nitrogen ($120 \text{ cm}^3 \text{ min}^{-1} \text{ g}^{-1}$). First the reactor was heated from room temperature to 473 K at 2 K min^{-1} and then from 473 K to 623 K at 3 K min^{-1} . The catalyst was kept at this final temperature for 3 h.

Material characterization

Argon physisorption isotherm measurements were performed on a Quantasorb Autosorb AS-1 (*Quantachrome Instruments*, USA) at 87.45 K or 77.3 K. Pore size distribution was determined from the adsorption branch of the isotherm, using the NLDFT software of Quantasorb assuming spherical/cylindrical pores in silica/zeolite.^[37] Samples are evacuated overnight at 623 K (heating rate of 2 K min^{-1}) under flowing N_2 ($120 \text{ cm}^3 \text{ min}^{-1} \text{ g}^{-1}$), followed by storage under Ar atmosphere. Prior to the sorption measurement, the samples are outgassed again under vacuum ($< 1 \text{ Pa}$) at 573 K (heating rate of 2 K min^{-1}).

Nitrogen physisorption was performed at 77 K on a *Micromeritics* TriStar instrument, controlled by TriStar 3000 software (*Micromeritics*) (version 6.03). Before measurement, samples are dried at 573 K (heating rate of 5 K min^{-1}) during 1000 min using a SmartPrep Programmable Degas System (*Micromeritics*). The t-plot was used for distinction between micro- and mesopores (thickness range = 0.35 – 0.50 nm).

Powder X-Ray Diffraction (XRD) patterns were recorded at room temperature on a STOE STADI MP diffractometer with focusing Ge(111) monochromator ($\text{CuK}\alpha_1$ radiation, $\lambda = 1.5406 \text{ \AA}$) in Debye-Scherrer geometry with a linear position sensitive detector (PSD) with 6° 2θ window. Data were recorded in the 2θ range of 4 to 60.50° with a step width of 0.5° ,

internal PSD resolution 0.01° , and a counting time of 300 s per step. All samples were equilibrated above saturated NH_4Cl aqueous solution at relative humidity of 79 % prior to the XRD measurement in order to ensure identical hydration. The crystalline, Bragg scattering fraction for all samples was obtained by least-squares fit of the intensity of the measured diffractograms by simulated XRD patterns over the whole measured data range.

High Resolution-SEM images were obtained with a Nova NanoSEM 450 (*FEI, Hillsboro, OR*). Samples mounted on aluminum stubs were used without any further modification. Before mounting the powder on the stub, a pinch of sample powder was dispersed in pure acetone; then a drop of the slurry was casted on the stub and allowed to dry.

Samples for *Transmission Electron Microscopy (TEM)* characterization were prepared by crushing the powder in ethanol and depositing drops of the suspension on a copper grid covered with a holey carbon film. High-angle annular dark-field scanning transmission electron microscopy (HAADF-STEM) images were collected using an aberration corrected cubed *FEI Titan* microscope operated at 200 kV. The mesoporous samples were additionally visualized using electron tomography, performed by collecting a tilt series of 2-dimensional images using HAADF-STEM over an angular range of $\pm 74^\circ$ with a tilt increment of 2° . After alignment of the projection images, a 3-dimensional reconstruction was obtained using the simultaneous iterative reconstruction technique (SIRT)^[63] implemented in the *FEI Inspect3D* software.

ICP-AES was performed with a *Horiba Ultima* instrument. Ar is used as plasma source and carrier gas. Filtrate analysis after NH_4OH treatment is performed in a polypropylene recipient. Before measurement, the fluid sample is centrifugally filtered with a Microsep 1-kDa filter system (*Filtron*). To determine the Si and Al amount, the zeolite (50 mg) is mixed with nitrohydrochloric acid (0.5 cm^3) and HF (3 cm^3) in a polytetrafluorethene or a polypropylene recipient for Al and Si determination, respectively. This mixture is kept at 383 K for Al

determination and at room temperature for Si determination, during 1 h. Subsequently, the mixture is transferred to a polytetrafluorethene flask, and bi-distilled water (10 cm³) and boric acid (2.8 g) are added. When the boric acid is dissolved completely, the solution is diluted with water and homogenized. This solution can be used for the ICP-AES measurement or diluted first with HCl (0.37 %).

FTIR spectroscopy of KBr-based wafers (1 wt% sample loading) was performed under vacuum (4 mbar) with a *Bruker* IFS 66v/S spectrometer, equipped with a MCT detector (128 scans per spectrum, 4 cm⁻¹ resolution). *FTIR spectroscopy* of self-supported wafers was performed with a *Nicolet* 6700 spectrometer, equipped with a DTGS detector (256 scans per spectrum, 2 cm⁻¹ resolution). The calcined sample is pressed and shaped as a self-supported wafer (about 5 to 10 mg cm⁻²), which is positioned in a temperature-controlled vacuum IR-cell with ZnSe windows. A vacuum of 1 mbar is applied. Before measurement, the sample is dried at 673 K during 1 h. Subsequently, a spectrum was scanned at 423 K. Zeolite acid density was determined by FTIR-monitored adsorption of pyridine vapor. After saturation of the sample with pyridine at 323 K, the excess of pyridine is removed during a period of 20 min. Then, the sample is heated again at 5 K min⁻¹ to gradually desorb the pyridine at different temperatures (423 K, 523 K and 623 K). FTIR-spectra are scanned at 423 K after 20 min of desorption at each temperature. The FTIR spectra of adsorbed pyridine were corrected by subtracting the blank spectrum of the degassed and pyridine-free sample. The band intensities at 1545 and 1455 cm⁻¹, normalized for sample mass differences, were used to quantify Brønsted and Lewis acid density, respectively, using the integrated molar extinction coefficients proposed by Emeis.^[64]

Solid-state NMR spectra were measured at room temperature under magic angle spinning (MAS) conditions on a *Bruker* Avance-500 spectrometer operating at 130.320 and 99.351 MHz for ²⁷Al and ²⁹Si, respectively. Spectra were recorded with single 90° pulse for ²⁹Si (4.0

μs) or 15° pulse for ^{27}Al ($0.5 \mu\text{s}$), at a spinning rate of 10 kHz, using a repetition time of 215 s for ^{29}Si and 0.1 s for ^{27}Al . High power decoupling with ^1H rf strength of ca. 42 kHz was applied in the case of ^{29}Si . The chemical shifts were calibrated relative to external standards, tetramethylsilane for ^{29}Si and aqueous $\text{Al}(\text{NO}_3)_3$ (1 M) for ^{27}Al (set to $\delta = 0$ ppm in each case).

Used (coked) catalysts were characterized with *thermogravimetric analysis (TGA)* under O_2 using a Q500 TGA from TA. The following temperature program was applied: heating to 333 K (3 K min^{-1} ; 30 min isothermal) followed by heating to 1073 K (3 K min^{-1} ; 30 min isothermal). Before TGA analysis, coked catalysts were washed 3 times with hexane, and dried overnight at 373 K to remove adsorbed reactants/products. The same washing and drying procedure is applied on fresh catalysts, used as reference to determine weight loss. The amount of adsorbed coke is equal to the weight loss after the dehydration phase (ended at 373 K).

Catalytic testing

The isomerization of α -pinene was performed in a 50 cm^3 stirred batch Parr-reactor at 423 K under N_2 atmosphere (0.6 MPa at ambient temperature) and a stirring rate of 750 rpm. The reactor was loaded with α -pinene (20 g, *Sigma-Aldrich*) and calcined zeolite catalyst (0.35 g; dry and pelletized). Before heating, the reactor is flushed three times during 1 min with N_2 . Samples are taken at selected time intervals and analyzed on a HP 5890 Series II gas chromatograph with a 60 m x 0.32 mm HP-1 capillary column. The analysis starts at 348 K and the temperature is increased to 523 K at a rate of 3 K min^{-1} . Identification of the reaction products was performed using standards. Unidentified peaks were resolved with GC-MS analysis using an Agilent 6890 GC with a 30 m x 0.25 mm HP-1 MS Ultra Inert capillary column and an Agilent 5973 MS. In a regeneration experiment, the catalyst was separated after reaction, washed with hexane (3x), dried overnight at 373 K, and calcined under an oxygen flow ($120 \text{ cm}^3 \text{ min}^{-1}$) in a flow reactor. The following temperature program was

applied: heating to 473 K (2 K min⁻¹; 30 min isothermal) followed by heating to 773 K (3 K min⁻¹; 180 min isothermal). After this regeneration procedure, the catalyst was subjected to an identical reaction with the same catalyst/substrate ratio. For this regeneration experiment, a sample of the reaction mixture was taken after cooling down the reactor.

Conjugation of safflower oil (ethyl esters) at 453 K was carried out in a 100 cm³ Parr-autoclave with sampling device and under 0.35 MPa of N₂ under constant stirring (500 rpm). Activated Ru/USY catalyst (0.8 g, 0.5 wt% Ru, Ru/lipid = 0.0150 wt%; dry and pelletized) was added to safflower oil ethyl esters (40 g; Oleon) or safflower oil (27 g; Oleon). Samples were taken at selected time intervals. The fatty acid composition of (converted) safflower oil was determined by analyzing the corresponding fatty acid methyl esters obtained by methanolysis. In this reaction, a sample (0.3 cm³) is dissolved in diethylether (3 cm³) and reacted with a solution (3 cm³) of KOH (5 wt%) in methanol. After 10 min, octane (3 cm³) is added. The formed methyl esters migrate to the octane phase, which is subsequently washed three times with distilled water (3 cm³). The fatty acid methyl or ethyl esters were analyzed using a HP 6890 gas chromatograph with a split injection system (split ratio = 100:1) and N₂ as carrier gas. A 100 m CP-SIL 88 highly polar capillary column with an internal diameter of 0.25 mm and a film thickness of 0.2 μm was used for separation. Initially, the column temperature is kept at 453 K for 50 min, and then raised at 10 K min⁻¹ to 498 K and held there for 15 min. The FID detector used was kept at 553 K. Heptadecane was used as external standard. Most CLA isomers were identified based on retention times, using references from *Matreya LLC*. Other CLA isomers were identified based on literature data.

Supporting Information

Supporting Information is available from the Wiley Online Library or from the author.

Acknowledgements

We thank dr. M. Thommes and dr. K. Cychosz for numerous and helpful discussions on the correct evaluation of the Ar isotherms. I. Cuppens is acknowledged for ICP-AES analyses. Research is funded through a PhD grant to J.V.A. of the Agency for Innovation by Science and Technology in Flanders (IWT). A.P. acknowledges F.W.O.-Vlaanderen (Research Foundation Flanders) for a postdoctoral fellowship. E.G., C.K. and J.M. acknowledge the long-term structural funding by the Flemish Government (Methusalem). S.B. acknowledges the European Research Council for funding under the European Union's Seventh Framework Programme (FP7/2007-2013)/ERC grant agreement N°335078-COLOURATOMS. The authors are grateful for financial support by the Belgian government through Interuniversity Attraction Poles (IAP-PAI). We thank Oleon NV for supplying safflower oil.

Received: ((will be filled in by the editorial staff))

Revised: ((will be filled in by the editorial staff))

Published online: ((will be filled in by the editorial staff))

- [1] H. van Bekkum, E. M. Flanigen, P. A. Jacobs, J. C. Jansen, *Introduction to Zeolite Science and Practice*, Elsevier, Amsterdam **2001**.
- [2] V. Valtchev, G. Majano, S. Mintova, J. Pérez-Ramírez, *Chem. Soc. Rev.* **2013**, *42*, 263.
- [3] W. Vermeiren, J.-P. Gilson, *Top. Catal.* **2009**, *52*, 1131.
- [4] E. M. Flanigen, R. W. Broach, S. T. Wilson, in *Zeolites in Industrial Separation and Catalysis*, (Ed: S. Kulprathipanja), Wiley-VCH Weinheim, Germany **2010**, Ch. 1.
- [5] J. Weitkamp, *Solid State Ionics* **2000**, *131*, 175.
- [6] P. A. Jacobs, M. Dusselier, B. F. Sels, *Angew. Chem. Int. Ed.* **2014**, *53*, 2; T. Ennaert, J. Geboers, E. Gobechiya, C. M. Courtin, M. Kurttepli, K. Houthoofd, C. E. A. Kirschhock, P. Magusin, S. Bals, P. A. Jacobs, B. F. Sels, *ACS Catal.* **2015**, *5*, 754; J. Geboers, S. Van de Vyver, K. Carpentier, P. Jacobs, B. Sels, *Chem. Comm.* **2011**, *47*, 5590; J. Čejka, G. Centi, J. Perez-Pariante, W. J. Roth, *Catal. Today* **2012**, *179*, 2; J. Dijkmans, M. Dusselier, D. Gabriels, K. Houthoofd, P. C. M. M. Magusin, S. Huang, Y. Pontikes, M. Trekels, A. Vantomme, L. Giebeler, S. Oswald, B. F. Sels, *ACS Catal.* **2015**, *5*, 928; J. Dijkmans, D. Gabriels, M. Dusselier, F. de Clippel, P. Vanelderden, K. Houthoofd, A. Malfliet, Y. Pontikes, B. F. Sels, *Green Chem.* **2013**, *15*, 2777; Y.-C. Lin, G. W. Huber, *Energy Environ. Sci.* **2009**, *2*, 68; G. W. Huber, A. Corma, *Angew. Chem. Int. Ed.* **2007**, *46*, 7184; E. Taarning, C. M. Osmundsen, X. Yang, B. Voss, S. I. Andersen, C. H. Christensen, *Energy Environ. Sci.* **2011**, *4*, 793; P. P. Pescarmona, K. P. F. Janssen, C. Delaet, C. Stroobants, K. Houthoofd, A. Philippaerts, C. De Jonghe, J. S. Paul, P. A. Jacobs, B. F. Sels, *Green Chem.* **2010**, *12*, 1083; R. Gounder, M. E. Davis, *J. Catal.* **2013**, *308*, 176; W. R. Gunther, Y. Wang, Y. Ji, V. K. Michaelis, S. T. Hunt, R. G. Griffin, Y. Román-Leshkov, *Nat. Commun.* **2012**, *3*, 1109; Y. Román-Leshkov, M. Moliner, J. A. Labinger, M. E. Davis, *Angew. Chem. Int. Ed.* **2010**, *49*, 8954; P. Y. Dapsens, B. T. Kusema, C. Mondelli, J. Pérez-Ramírez, *J. Mol. Catal. A: Chem.* **2014**, *388–389*, 141; P.

- Y. Dapsens, M. J. Menart, C. Mondelli, J. Pérez-Ramírez, *Green Chem.* **2014**, *16*, 589; C. Zhao, J. A. Lercher, *ChemCatChem* **2012**, *4*, 64; C. Zhao, J. A. Lercher, *Angew. Chem. Int. Ed.* **2012**, *51*, 5935; C. Zhao, W. Song, J. A. Lercher, *ACS Catal.* **2012**, *2*, 2714; B. Peng, Y. Yao, C. Zhao, J. A. Lercher, *Angew. Chem. Int. Ed.* **2012**, *51*, 2072.
- [7] N. Nuttens, D. Verboekend, A. Deneyer, J. Van Aelst, B. F. Sels, *ChemSusChem*, DOI: 10.1002/cssc.201403457.
- [8] D. Kubička, I. Kubičková, J. Čejka, *Catal. Rev.* **2013**, *55*, 1; D. Kubička, O. Kikhtyanin, *Catal. Today* **2015**, *243*, 10.
- [9] M. Davis, E., *Nature* **2002**, *417*, 813.
- [10] J. Pérez-Ramírez, C. H. Christensen, K. Egeblad, C. H. Christensen, J. C. Groen, *Chem. Soc. Rev.* **2008**, *37*, 2530.
- [11] J. A. Martens, D. Verboekend, K. Thomas, G. Vanbutsele, J. Pérez-Ramírez, J.-P. Gilson, *Catal. Today* **2013**, *218–219*, 135; J. A. Martens, D. Verboekend, K. Thomas, G. Vanbutsele, J.-P. Gilson, J. Pérez-Ramírez, *ChemSusChem* **2013**, *6*, 421.
- [12] P. Y. Dapsens, C. Mondelli, J. Pérez-Ramírez, *ACS Catal.* **2012**, *2*, 1487.
- [13] A. Corma, M. J. Diaz-Cabanas, F. Rey, S. Nicolopoulos, K. Boulahya, *Chem. Comm.* **2004**, 1356; A. Corma, M. Diaz-Cabanas, J. Martinez-Triguero, F. Rey, J. Rius, *Nature* **2002**, *418*, 514; M. E. Davis, C. Saldarriaga, C. Montes, J. Garces, C. Crowder, *Nature* **1988**, *331*, 698; J. Jiang, J. Yu, A. Corma, *Angew. Chem. Int. Ed.* **2010**, *49*, 3120.
- [14] S. C. Larsen, *J. Phys. Chem. C* **2007**, *111*, 18464; W. J. Roth, J. Cejka, *Catal. Sci. Technol.* **2011**, *1*, 43; H. Awala, J.-P. Gilson, R. Retoux, P. Boullay, J.-M. Goupil, V. Valtchev, S. Mintova, *Nat. Mater.* **2015**, *14*, 447; M. Choi, K. Na, J. Kim, Y. Sakamoto, O. Terasaki, R. Ryoo, *Nature* **2009**, *461*, 246; Z. Qin, L. Lakiss, L. Tosheva, J.-P. Gilson, A. Vicente, C. Fernandez, V. Valtchev, *Adv. Funct. Mater.* **2014**, *24*, 257.
- [15] D. Verboekend, J. Pérez-Ramírez, *ChemSusChem* **2014**, *7*, 753.
- [16] S. Lopez-Orozco, A. Inayat, A. Schwab, T. Selvam, W. Schwieger, *Adv. Mater.* **2011**, *23*, 2602; D. P. Serrano, J. M. Escola, P. Pizarro, *Chem. Soc. Rev.* **2013**, *42*, 4004; R. Chal, C. Gérardin, M. Bulut, S. van Donk, *ChemCatChem* **2011**, *3*, 67; F.-S. Xiao, X. Meng, in *Hierarchically Structured Porous Materials*, (Eds: B.-L. Su, C. Sanchez, X.-Y. Yang), Wiley-VCH Weinheim, Germany **2012**, Ch. 14; K. Moller, T. Bein, *Chem. Soc. Rev.* **2013**, *42*, 3689.
- [17] Z. L. Hua, J. Zhou, J. L. Shi, *Chemical Communications* **2011**, *47*, 10536.
- [18] D. Verboekend, J. Pérez-Ramírez, *Catal. Sci. Technol.* **2011**, *1*, 879; D. Zhai, L. Zhao, Y. Liu, J. Xu, B. Shen, J. Gao, *Chem. Mater.* **2014**, DOI: 10.1021/cm503151k.
- [19] D. Verboekend, T. C. Keller, M. Milina, R. Hauert, J. Pérez-Ramírez, *Chem. Mater.* **2013**, *25*, 1947.
- [20] J. C. Groen, L. A. A. Peffer, J. A. Moulijn, J. Pérez-Ramírez, *Chem. Eur. J.* **2005**, *11*, 4983; J. Groen, T. Sano, J. Moulijn, J. Pérez-Ramírez, *J. Catal.* **2007**, *251*, 21; J. C. Groen, S. Abello, L. A. Villaescusa, J. Pérez-Ramírez, *Micropor. Mesopor. Mat.* **2008**, *114*, 93; D. Verboekend, M. Milina, J. Pérez-Ramírez, *Chem. Mater.* **2014**, *26*, 4552; J. Pérez-Ramírez, D. Verboekend, A. Bonilla, S. Abelló, *Adv. Funct. Mater.* **2009**, *19*, 3972; D. Verboekend, T. C. Keller, S. Mitchell, J. Pérez-Ramírez, *Adv. Funct. Mater.* **2013**, *23*, 1923; D. Verboekend, J. C. Groen, J. Pérez-Ramírez, *Adv. Funct. Mater.* **2010**, *20*, 1441.
- [21] D. Verboekend, S. Mitchell, M. Milina, J. C. Groen, J. Pérez-Ramírez, *J. Phys. Chem. C* **2011**, *115*, 14193.
- [22] K. P. de Jong, Zecevic, J., Friedrich, H., de Jongh, P.E., Bulut, M., van Donk, S., Kenmogne, R., Finiels, A., Hulea, V., Fajula, F., *Angew. Chem. Int. Ed.* **2010**, *122*, 10272.
- [23] D. Verboekend, G. Vilé, J. Pérez-Ramírez, *Adv. Funct. Mater.* **2012**, *22*, 916.
- [24] D. Verboekend, G. Vilé, J. Pérez-Ramírez, *Cryst. Growth Des.* **2012**, *12*, 3123.
- [25] J. C. Groen, J. A. Moulijn, J. Pérez-Ramírez, *Ind. Eng. Chem. Res.* **2007**, *46*, 4193.
- [26] H. Matsuura, N. Katada, M. Niwa, *Micropor. Mesopor. Mat.* **2003**, *66*, 283.

- [27] J. García-Martínez, M. Johnson, J. Valla, K. Li, J. Y. Ying, *Catal. Sci. Technol.* **2012**, *2*, 987.
- [28] D. Verboekend, M. Milina, S. Mitchell, J. Pérez-Ramírez, *Cryst. Growth Des.* **2013**, *13*, 5025.
- [29] A. Philippaerts, J. Geboers, S. Goossens, B. Sels *WO2012068645*, **2010**.
- [30] J. Van Aelst, M. Haouas, E. Gobechiya, K. Houthoofd, A. Philippaerts, S. P. Sree, C. E. A. Kirschhock, P. Jacobs, J. A. Martens, B. F. Sels, F. Taulelle, *J. Phys. Chem. C* **2014**, *118*, 22573.
- [31] Y. Wu, F. Tian, J. Liu, D. Song, C. Jia, Y. Chen, *Micropor. Mesopor. Mat.* **2012**, *162*, 168.
- [32] A. Corma, S. Iborra, A. Velty, *Chem. Rev.* **2007**, *107*, 2411.
- [33] P. Mäki - Arvela, B. Holmbom, T. Salmi, D. Y. Murzin, *Catal. Rev.* **2007**, *49*, 197; K. Swift, *Top. Catal.* **2004**, *27*, 143; J. Monteiro, *Top. Catal.* **2004**, *27*, 169; N. Ravasio, *Top. Catal.* **2004**, *27*, 157.
- [34] A. Philippaerts, S. Goossens, P. A. Jacobs, B. F. Sels, *ChemSusChem* **2011**, *4*, 684; A. Philippaerts, J. Van Aelst, B. Sels, *Eur. J. Lipid. Sci. Tech.* **2013**, *115*, 717; B. Sels, A. Philippaerts, *Conjugated Linoleic Acids and Conjugated Vegetable Oils*, Royal Society of Chemistry, Abingdon, Oxfordshire, UK **2014**.
- [35] A. Philippaerts, S. Goossens, W. Vermandel, M. Tromp, S. Turner, J. Geboers, G. Van Tendeloo, P. A. Jacobs, B. F. Sels, *ChemSusChem* **2011**, *4*, 757.
- [36] M. Thommes, in *Studies in Surface Science and Catalysis*, Vol. 168 (Eds: J. Čejka, H. v. Bekkum, A. Corma, F. Schüth), Elsevier, Oxford, UK **2007**, Ch. 15.
- [37] J. Landers, G. Y. Gor, A. V. Neimark, *Colloid Surface A* **2013**, *437*, 3.
- [38] M. Thommes, *Chem.-Ing.-Tech.* **2010**, *82*, 1059.
- [39] J. Garcia-Martinez, C. Xiao, K. A. Cychosz, K. Li, W. Wan, X. Zou, M. Thommes, *ChemCatChem* **2014**, *6*, 3110.
- [40] M. Thommes, R. Köhn, M. Fröba, *Appl. Surf. Sci.* **2002**, *196*, 239.
- [41] A. H. Janssen, A. J. Koster, K. P. de Jong, *J. Phys. Chem. B* **2002**, *106*, 11905; H. Giesche, *Part. Part. Syst. Char.* **2006**, *23*, 9.
- [42] J. Zečević, C. J. Gommès, H. Friedrich, P. E. de Jongh, K. P. de Jong, *Angew. Chem. Int. Ed.* **2012**, *51*, 4213.
- [43] A. J. M. de Man, R. A. van Santen, *Zeolites* **1992**, *12*, 269; J. Scherzer, J. L. Bass, *J. Catal.* **1973**, *28*, 101; L. Can, W. Zili, in *Handbook of Zeolite Science and Technology*, (Eds: S. M. Auerbach, K. A. Carrado, P. K. Dutta), Marcel Dekker, New York, USA **2003**, Ch. 11.
- [44] J. W. Ward, *J. Catal.* **1967**, *9*, 225.
- [45] R. S. McDonald, *J. Phys. Chem.* **1958**, *62*, 1168.
- [46] IZA, Database of Zeolite Structures, <http://www.iza-structure.org/databases/>, accessed: March, 2015.
- [47] O. Cairon, *ChemPhysChem* **2013**, *14*, 244.
- [48] J. Klinowski, *Prog. Nucl. Mag. Res. Sp.* **1984**, *16*, 237; J. Klinowski, J. M. Thomas, C. A. Fyfe, G. C. Gobbi, *Nature* **1982**, *296*, 533; G. Engelhardt, D. Michel, *High-Resolution Solid-State NMR of Silicates and Zeolites*, John Wiley & Sons, Chichester, UK **1987**.
- [49] M. J. Remy, D. Stanica, G. Poncelet, E. J. P. Feijen, P. J. Grobet, J. A. Martens, P. A. Jacobs, *J. Phys. Chem.* **1996**, *100*, 12440.
- [50] A. Samoson, E. Lippmaa, G. Engelhardt, U. Lohse, H. G. Jerschke, *Chem. Phys. Lett.* **1987**, *134*, 589; H. Kosslick, V. A. Tuan, R. Fricke, A. Martin, W. Storek, in *Studies in Surface Science and Catalysis*, Vol. 84 (Eds: J. Weitkamp, H. G. Karge, H. Pfeifer, W. Hölderich), Elsevier, Oxford, UK **1994**, p. 1013; P. J. Grobet, H. Geerts, M. Tielen, J. A. Martens, P. A. Jacobs, in *Studies in Surface Science and Catalysis*, Vol. 46 (Eds: H. G. Karge, J. Weitkamp), Elsevier, Oxford, UK **1989**, p. 721; Z. Yan, D. Ma, J. Zhuang, X. Liu, X. Liu,

- X. Han, X. Bao, F. Chang, L. Xu, Z. Liu, *J. Mol. Catal. A* **2003**, *194*, 153; Z. Yu, A. Zheng, Q. Wang, L. Chen, J. Xu, J.-P. Amoureux, F. Deng, *Angew. Chem. Int. Ed.* **2010**, *49*, 8657.
- [51] A. W. Peters, C. C. Wu, *Catal. Lett.* **1995**, *30*, 171.
- [52] D. Verboekend, J. Pérez-Ramírez, *Chem. Eur. J.* **2011**, *17*, 1137.
- [53] D. Verboekend, A. M. Chabaneix, K. Thomas, J.-P. Gilson, J. Pérez-Ramírez, *CrystEngComm* **2011**, *13*, 3408.
- [54] C. J. Brinker, G. W. Scherer, *Sol-Gel Science*, Elsevier, Oxford, UK **1990**.
- [55] P. G. Smirniotis, L. E. V. Davydov, E. L. I. Ruckenstein, *Catal. Rev.* **1999**, *41*, 43.
- [56] J. M. Maselli, A. W. Peters, *Catal. Rev.* **1984**, *26*, 525.
- [57] R. Rachwalik, M. Hunger, B. Sulikowski, *Appl. Catal. A: Gen.* **2012**, *427-428*, 98; C. M. López, F. J. Machado, K. Rodríguez, B. Méndez, M. Hasegawa, S. Pekarar, *Appl. Catal. A: Gen.* **1998**, *173*, 75; A. Severino, A. Esculcas, J. Rocha, J. Vital, L. S. Lobo, *Appl. Catal. A: Gen.* **1996**, *142*, 255; Ł. Mokrzycki, B. Sulikowski, Z. Olejniczak, *Catal. Lett.* **2008**, *127*, 296; F. Tian, Y. Wu, Q. Shen, X. Li, Y. Chen, C. Meng, *Micropor. Mesopor. Mat.* **2013**, *173*, 129; J. Wang, W. Hua, Y. Yue, Z. Gao, *Bioresource Technol.* **2010**, *101*, 7224; B. Gil, Ł. Mokrzycki, B. Sulikowski, Z. Olejniczak, S. Walas, *Catal. Today* **2010**, *152*, 24.
- [58] N. Flores-Holguín, A. Aguilar-Elguézabal, L. M. Rodríguez-Valdez, D. Glossman-Mitnik, *J. Mol. Struc.-THEOCHEM* **2008**, *854*, 81; F. Ebmeyer, *J. Mol. Struc.-THEOCHEM* **2002**, *582*, 251.
- [59] D. M. Roberge, D. Buhl, J. P. M. Niederer, W. F. Hölderich, *Appl. Catal. A: Gen.* **2001**, *215*, 111.
- [60] M. S. Holm, E. Taarning, K. Egeblad, C. H. Christensen, *Catal. Today* **2011**, *168*, 3.
- [61] M. W. Pariza, Y. Park, M. E. Cook, *Prog. Lipid. Res.* **2001**, *40*, 283; B. Szymczyk, P. M. Pisulewski, W. Szczurek, P. Hanczakowski, *British J. Nutr.* **2001**, *85*, 465; M. A. Latour, A. A. Devitt, R. A. Meunier, J. J. Stewart, B. A. Watkins, *Poultry Sci.* **2000**, *79*, 817; R. G. Twibell, B. A. Watkins, L. Rogers, P. B. Brown, *Lipids* **2000**, *35*, 155; E. Ostrowska, M. Muralitharan, R. F. Cross, D. E. Bauman, F. R. Dunshea, *J. Nutr.* **1999**, *129*, 2037.
- [62] T. F. Bradley *US2350583*, **1944**; G. S. Penumarti, S. A. Joti *US2749247*, **1956**; I. J. Novak *US2318009*, **1943**; R. T. Sleeter *CA 2178437*, **2005**.
- [63] P. Gilbert, *J. Theor. Biol.* **1972**, *36*, 105.
- [64] C. A. Emeis, *J. Catal.* **1993**, *141*, 347.

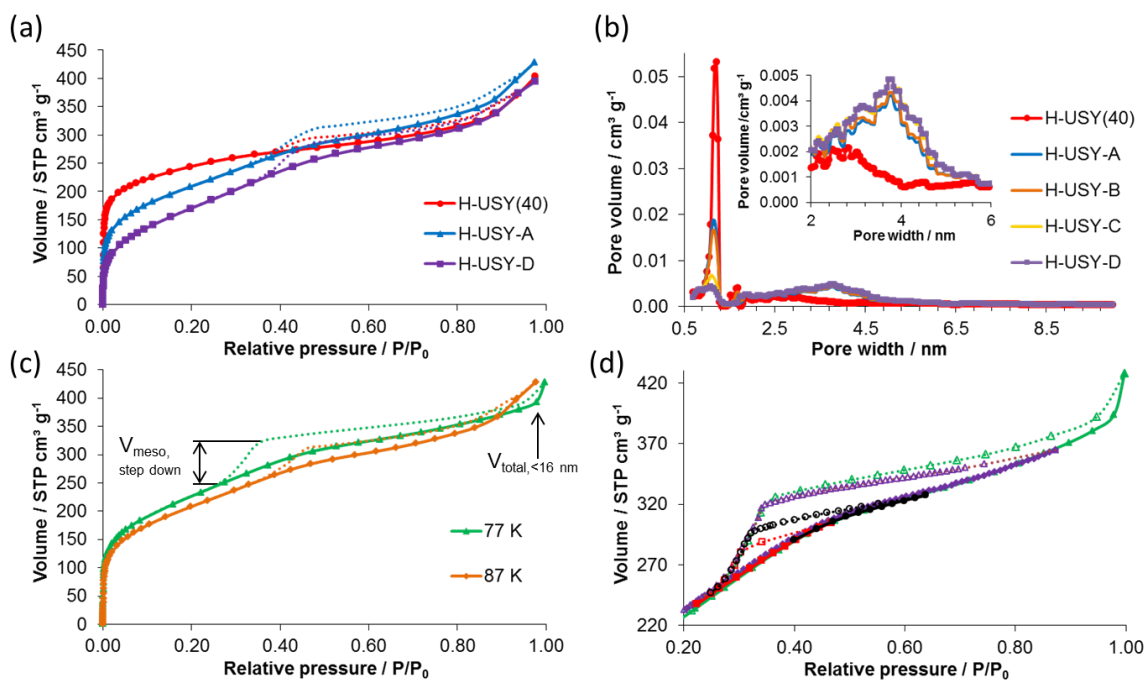


Figure 1. (a) Ar physisorption (87 K) isotherms with adsorption (full line) and desorption curve (dotted line) for H-USY(40), H-USY-A and H-USY-D samples. (b) Pore size distributions (NLDFT model) determined from the Ar adsorption isotherm for all studied samples, the inset depicting the distribution of pores with a diameter of 2-6 nm. (c) Ar physisorption isotherms for H-USY-B at 87 K and 77 K. (d) Hysteresis scanning for H-USY-B at 77 K.

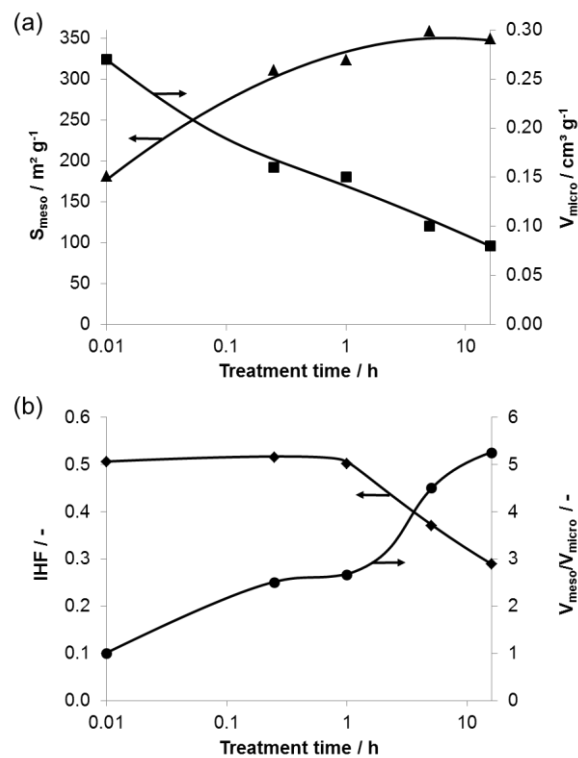


Figure 2. (a) Evolution of specific mesoporous surface area S_{meso} and specific microporous volume V_{micro} in function of NH_4OH treatment time. (b) Evolution of indexed hierarchy factor (IHF) and the ratio of specific mesoporous volume V_{meso} to specific microporous volume V_{micro} in function of NH_4OH treatment time.

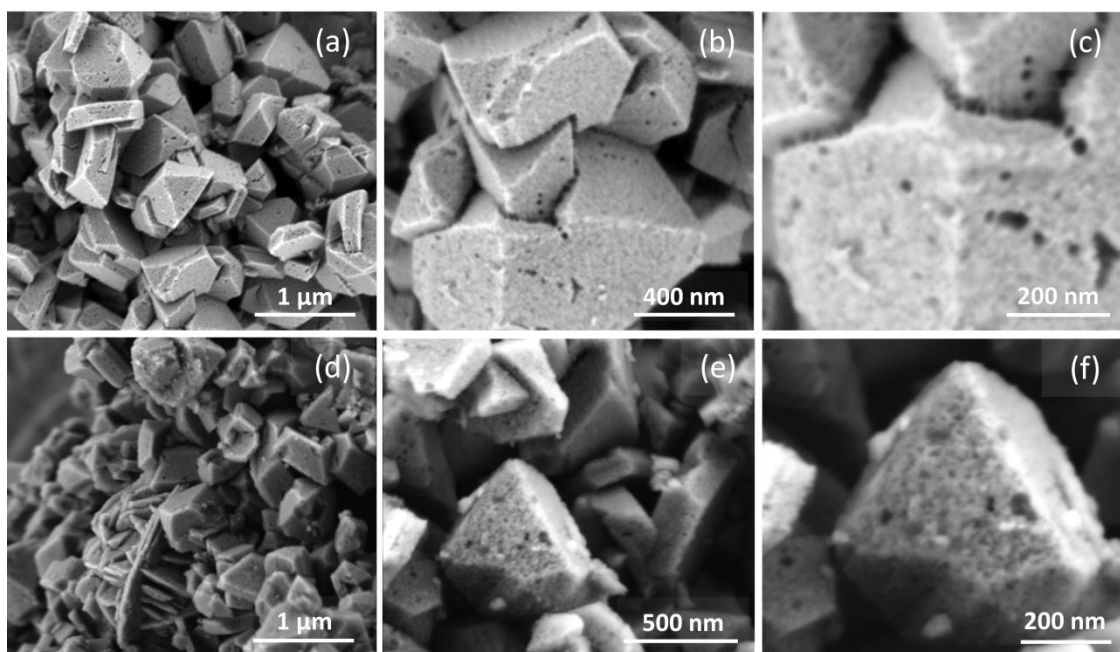


Figure 3. HR-SEM images with various magnifications of H-USY(40) (a-c) and H-USY-D samples (d-f).

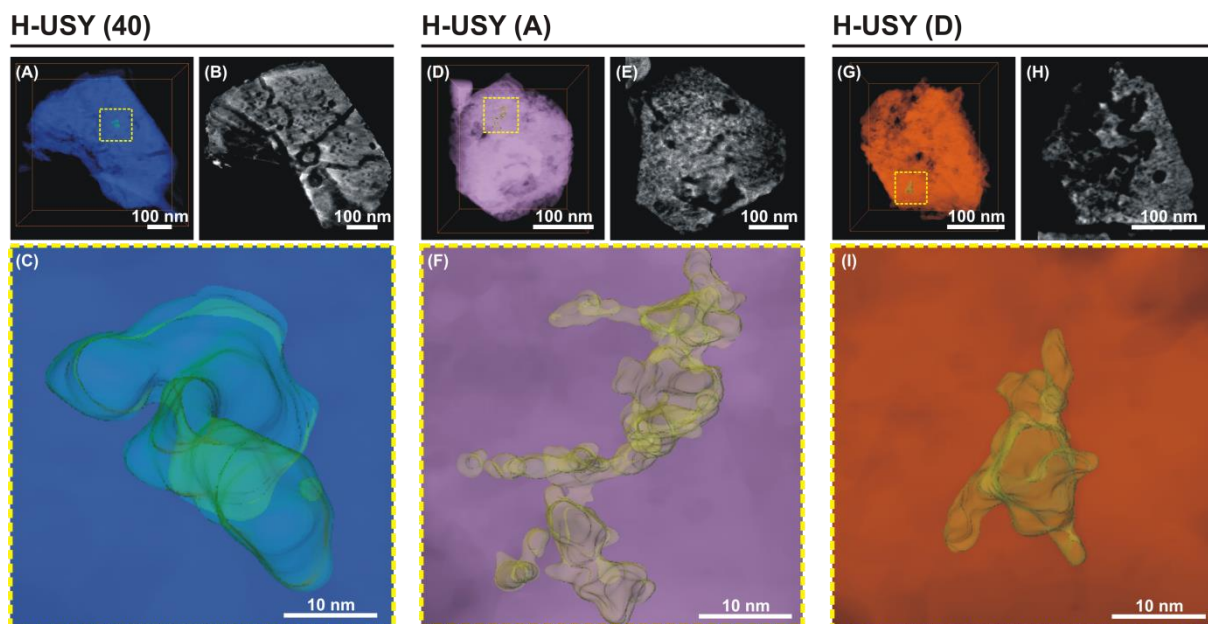


Figure 4. Visualizations of representative crystals of (a) H-USY(40), (d) H-USY-A and (g) H-USY-D made by 3-D reconstruction of HAADF-STEM orthoslices ((b), (e), (h)). Representative pores for the different samples, as indicated in (a), (d) and (g) are presented in (c), (f) and (i).

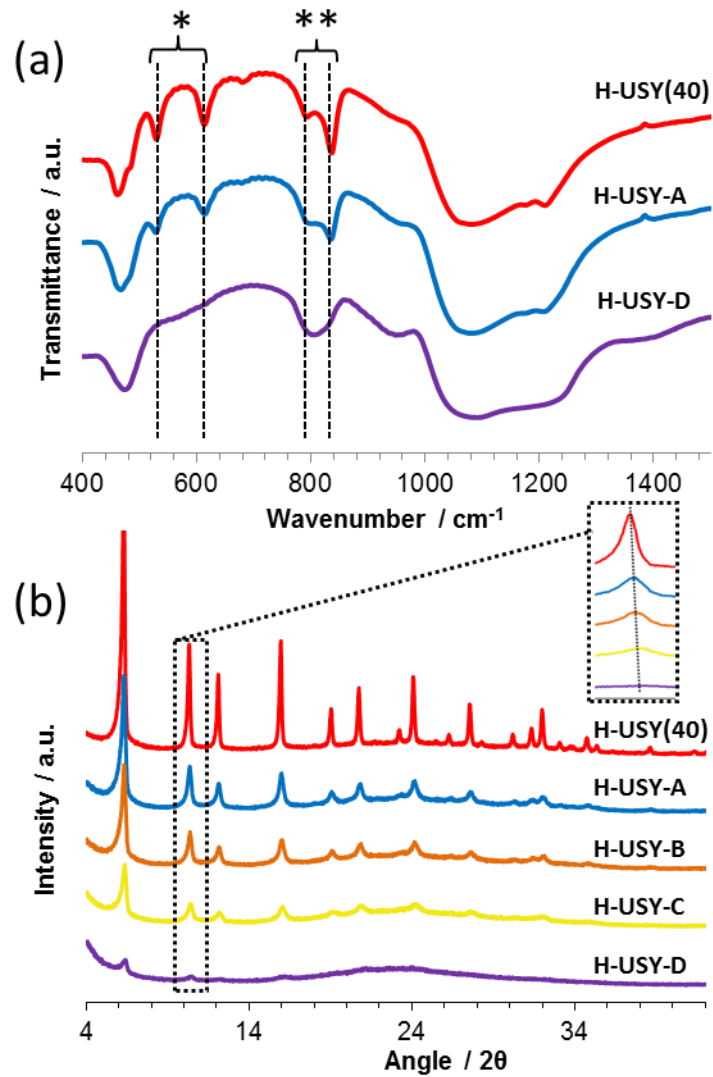


Figure 5. (a) FTIR-spectra of framework vibrations for samples H-USY(40), H-USY-A and H-USY-D (*, stretching vibrations of double six-membered rings (D6R); **, symmetrical stretching mode of zeolite TO_4 tetrahedra). (b) XRD patterns for all studied samples, including inset which indicates the gradual peak shift.

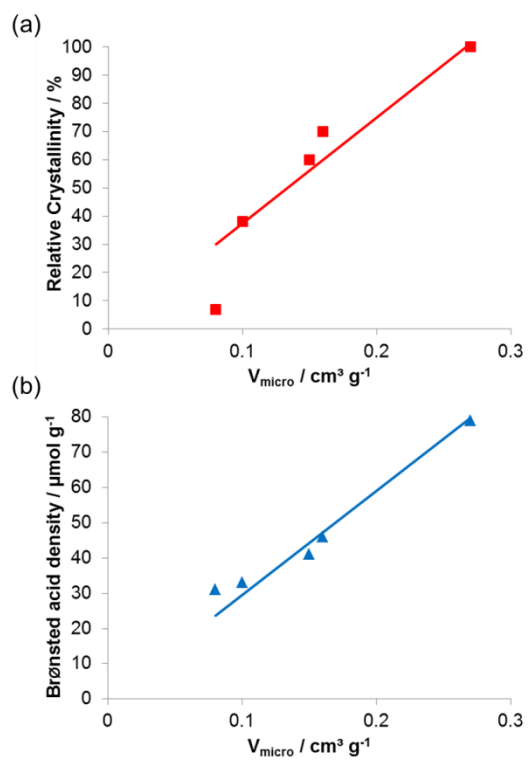
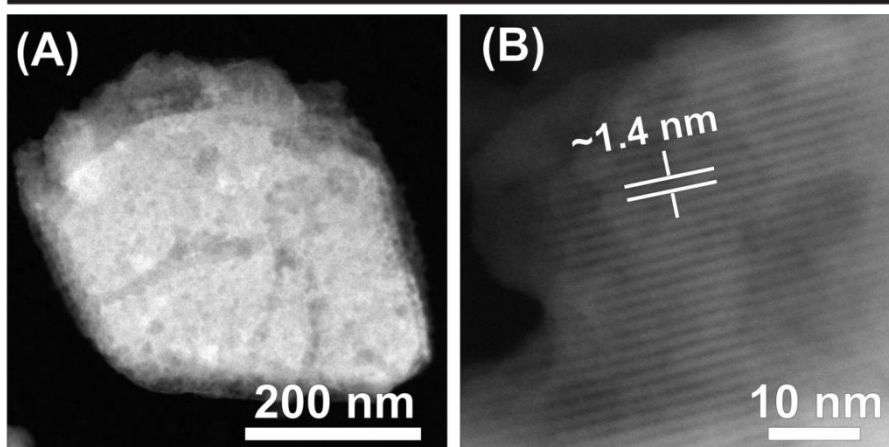
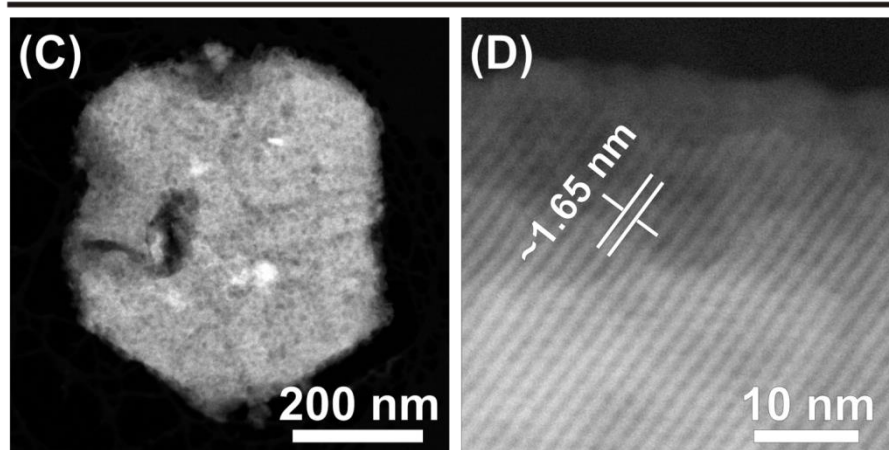


Figure 6. Correlation of microporous volume V_{micro} with (a) relative crystallinity and (b) Brønsted acid density.

H-USY (40)



H-USY (A)



H-USY (D)

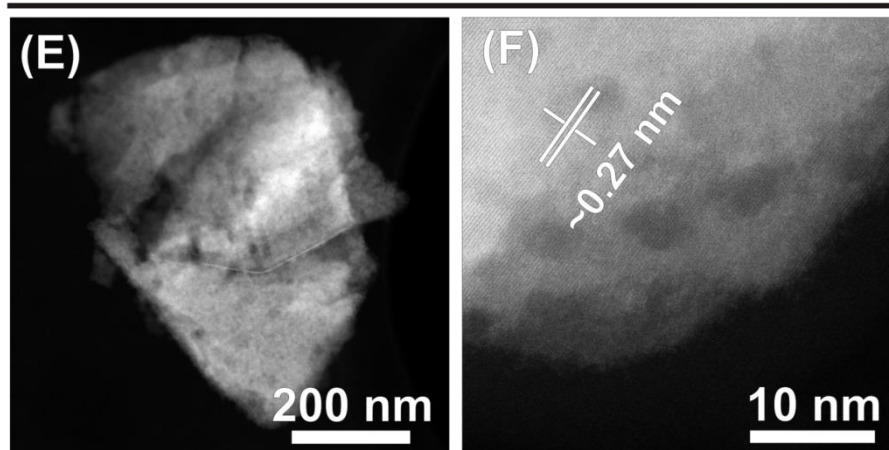


Figure 7. HAADF-STEM images for H-USY(40) (a-b), H-USY-A (c-d) and H-USY-D (e-f) samples additionally reveal sample porosity and crystallinity, respectively. The micrographs (b), (d) and (f) show the presence of lattice fringes.

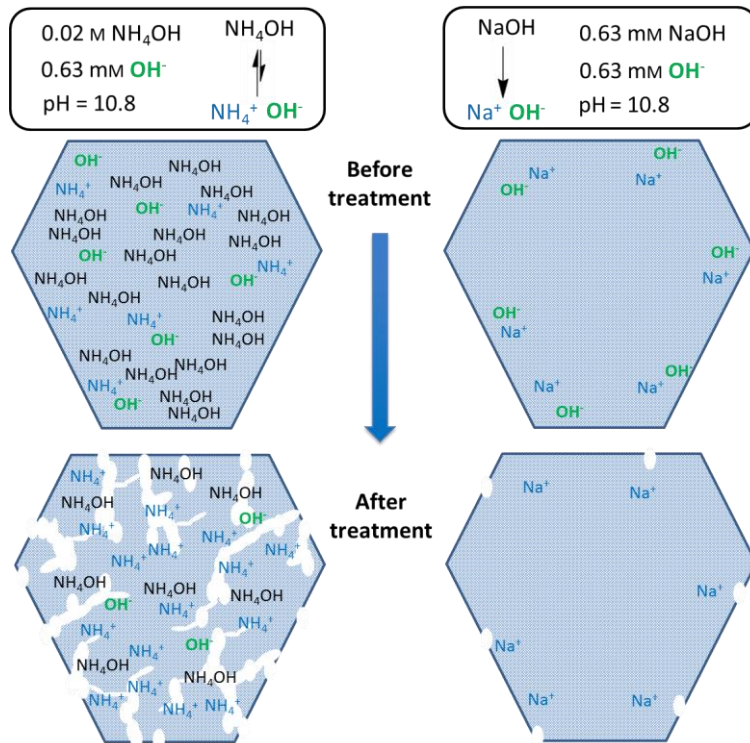


Figure 8. Schematic representation of the intracrystalline fluids concentration in USY crystals during the alkaline treatment with a weak (NH_4OH) and a strong (NaOH) base at an initial pH of 10.8. For clarity reasons, the original mesoporosity already present before treatment is not shown.

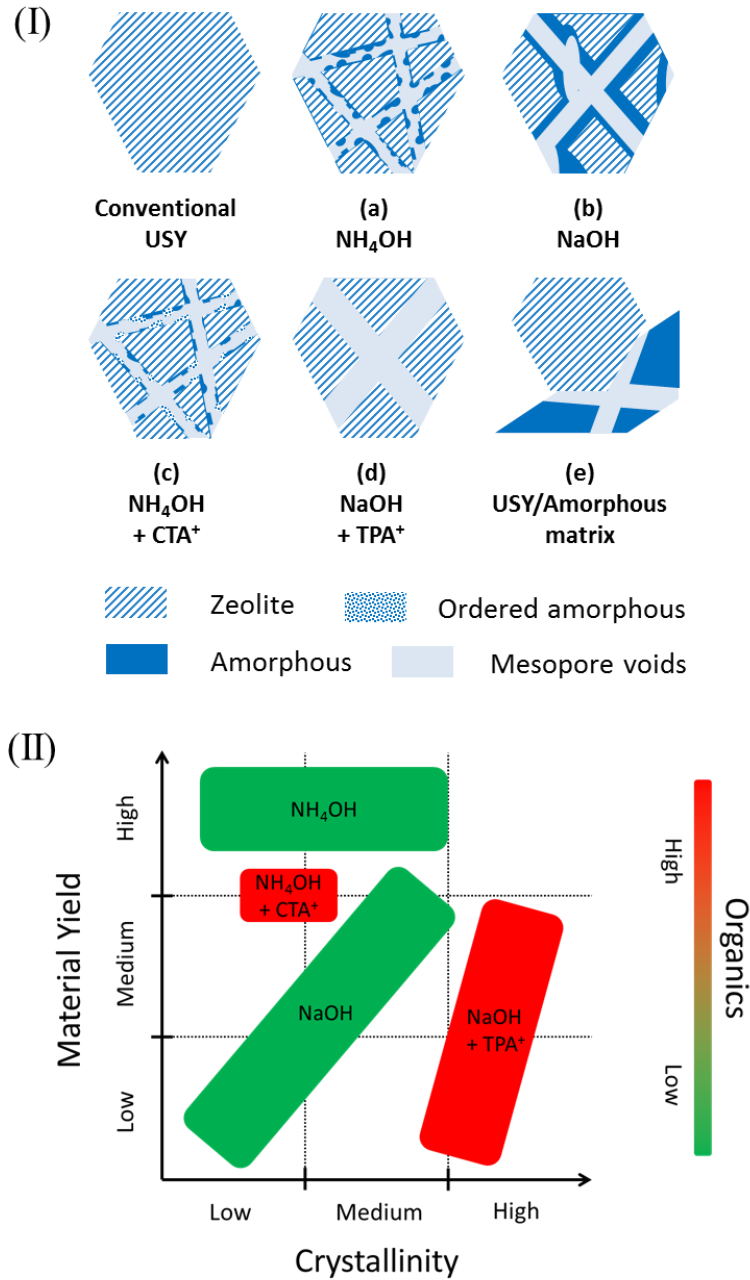


Figure 9. (I). Overview of different alkaline treatments of USY (a-d) and comparison with addition of extracrystalline amorphous silica-alumina (e), and (II). qualitative evaluation of the crystallinity, material yield and load of organics needed. For clarity reasons, the original mesoporosity already present before treatment in the conventional USY is not shown.

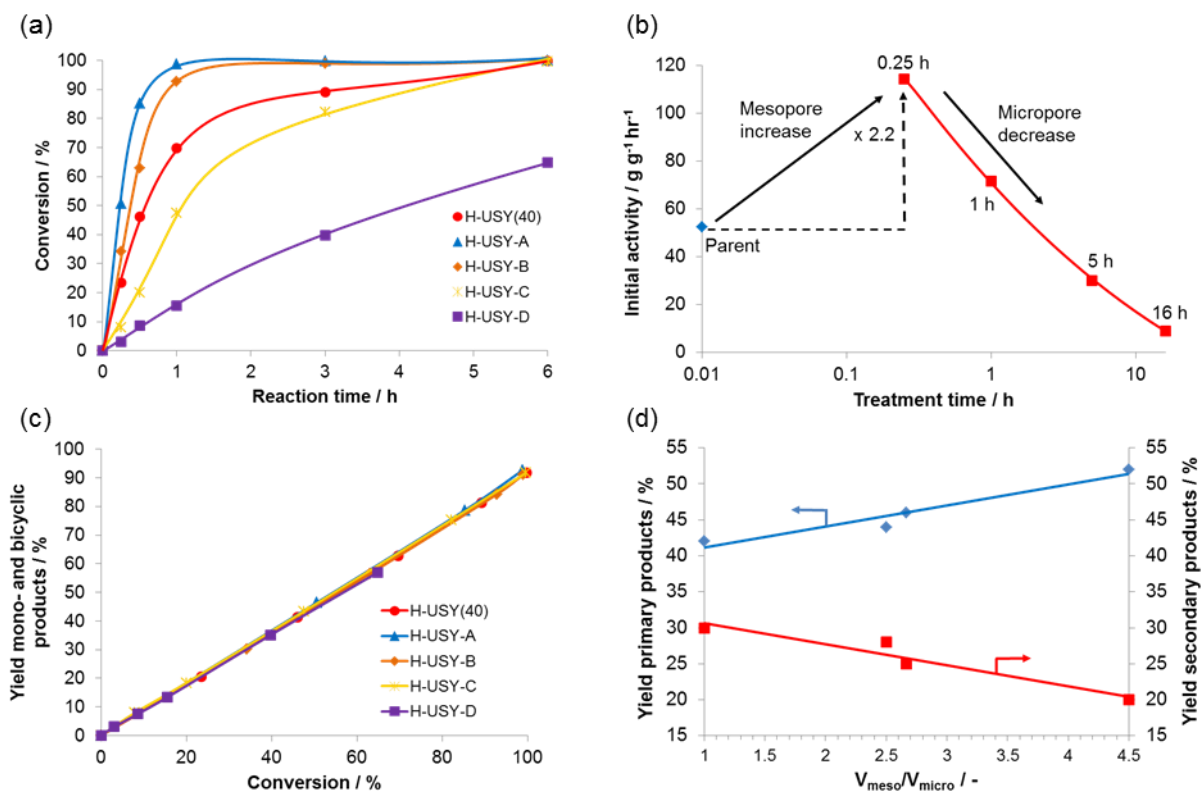


Figure 10. α -Pinene isomerization on H-USY-40 and all NH₄OH treated samples; (a) α -pinene conversion in function of reaction time; (b) Evolution of the initial activity in function of the NH₄OH treatment time for all studied samples (logarithmic; treatment time of parent set at 0.01 h); (c) Yield of mono- and bicyclic α -pinene-derived products, *i.e.* camphene, limonene, α -terpinene, γ -terpinene, terpinolene, p-cymene, tricyclene, p-menthene and 3,8-p-menthadiene, in function of α -pinene conversion; (d) Correlation of the yield of respectively primary and secondary formed products (determined at an isoconversion of 80 %) with the V_{meso}/V_{micro} ratio.

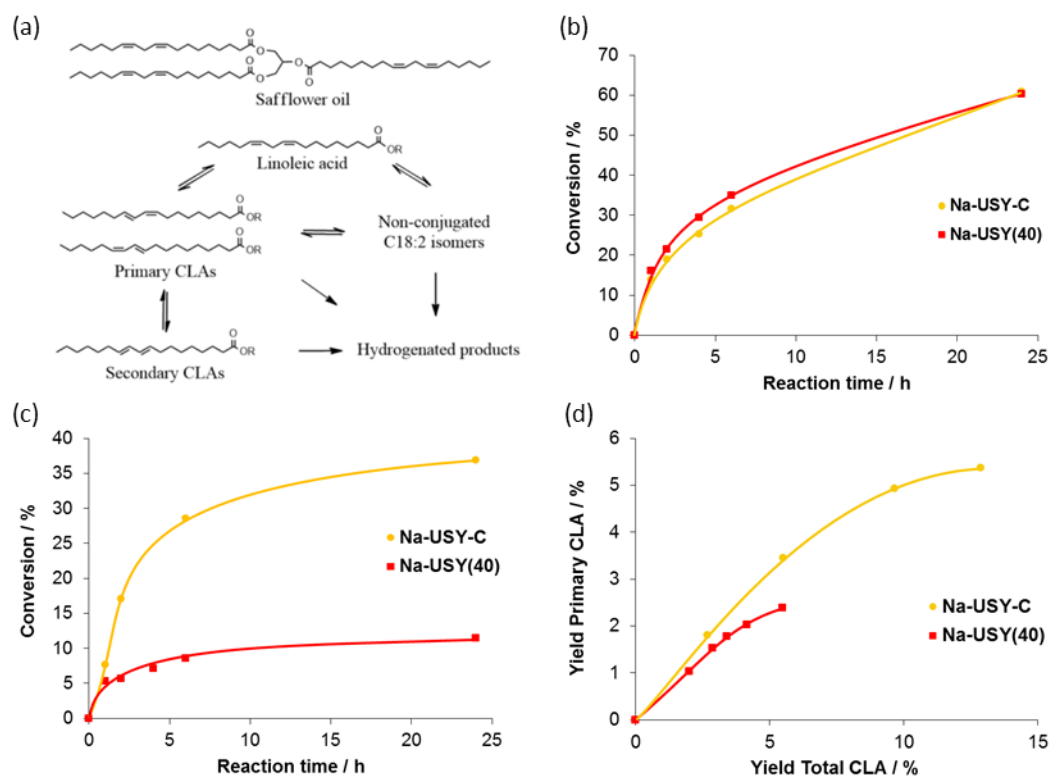


Figure 11. Effect of USY zeolite hierarchization with NH_4OH on conjugation of safflower oil and its corresponding ethyl esters: (a) structure of typical triglyceride in safflower oil and general reaction scheme for conjugation of linoleic acid, depicted here as being esterified to the ethyl group R or the remaining diglyceride R, respectively for the conjugation of safflower oil ethyl esters and safflower oil. This conjugation reaction produces conjugated linoleic acid (CLA), forming both primary (kinetically favored) and secondary (thermodynamically favored) CLA isomers; (b) Conjugation activity for linoleate present as ethyl ester at 453 K with Ru-loaded Na-USY(40) and Na-USY-C catalysts; (c) Conjugation activity for linoleate present as triglyceride at 453 K with Ru-loaded Na-USY(40) and Na-USY-C catalysts; (d) Primary CLA isomer yield against total CLA isomer yield for both catalysts.

Table 1. Overview of studied samples, before and after NH₄OH treatment for different contact times, showing in the left part quantification of the specific pore volumes (V_i) and specific surface areas (S_i) for the different pore types, determined by application of the NLDFT model on the Ar isotherms at 87 K. The subscripts *s-meso* and *meso* refer to small mesopores (2-6 nm) and total amount of mesopores, respectively. In the right part, specific pore volumes derived from the Ar isotherms at 77 K are given, as well as the calculated fraction of restricted mesopores (< 16 nm).

		87 K						77 K			
Sample	Treatment time (h)	V_{micro} [cm ³ g ⁻¹]	$V_{\text{s-meso}}$ [cm ³ g ⁻¹]	V_{meso} [cm ³ g ⁻¹]	V_{total} [cm ³ g ⁻¹]	S_{micro} [m ² g ⁻¹]	S_{meso} [m ² g ⁻¹]	$V_{\text{total}, < 16 \text{ nm}}^{\text{a)}}$ [cm ³ g ⁻¹]	$V_{\text{meso}, \text{step down}}^{\text{a)}}$ [cm ³ g ⁻¹]	$V_{\text{meso}, < 16 \text{ nm}}^{\text{a)}}$ [cm ³ g ⁻¹]	Restricted $V_{\text{meso}, < 16 \text{ nm}}$ [%]
H-USY(40)	-	0.27	0.11	0.27	0.53	1378	181	0.41	0.03	0.14	21
H-USY-A	0.25	0.16	0.22	0.40	0.55	844	311	0.42	0.09	0.26	35
H-USY-B	1.0	0.15	0.23	0.40	0.55	788	323	0.48	0.10	0.33	30
H-USY-C	5.0	0.10	0.26	0.45	0.54	541	358	0.42	0.10	0.32	31
H-USY-D	16.0	0.08	0.26	0.42	0.50	459	349	-	-	-	-

^{a)} determined applying the Gurvich rule.

Table 2. Overview of USY samples, before and after NH₄OH treatment for different contact times, showing relative XRD-crystallinity, Brønsted acid densities from FTIR monitored pyridine desorption at different temperatures, bulk Si/Al ratio and material yield.

Sample	Treatment time (h)	Relative crystallinity [%] ^{a)}	Brønsted acid density [$\mu\text{mol g}^{-1}$]			Si/Al ^{b)}	Yield [wt%]
			423 K	523 K	623 K		
H-USY(40)	-	100	79	77	66	47.5	-
H-USY-A	0.25	70	46	42	38	(47)	90
H-USY-B	1.0	60	41	41	39	(47)	91
H-USY-C	5.0	38	33	31	25	(47)	94
H-USY-D	16.0	7	31	27	16	46.7	93

^{a)} determined by XRD; ^{b)} determined by ICP-AES, values between brackets are based on ICP-AES measurements of the filtrate.

NH₄OH treatment is performed on USY zeolite to develop superior catalysts. Extensive characterization of the material obtained by this sustainable post-synthetic hierarchization method shows the selective creation of small mesopores. These were formed by partial zeolite densification without significant material leaching. The hierarchical zeolite outperforms the conventional USY for both acid-catalyzed isomerization of α -pinene and metal-catalyzed conjugation of safflower oil, which is attributed to its enhanced intracrystalline mass transport capacity.

Keywords: USY, hierarchical zeolite, NH₄OH, alkaline treatment, catalysis

*Joost Van Aelst, An Philippaerts, Nicolas Nuttens, Danny Verboekend, Mert Kurttepli, Elena Gobechiya, Mohamed Haouas, Sreeprasanth P. Sree, Joeri F. M. Denayer, Johan A. Martens, Christine E. A. Kirschhock, Francis Taulelle, Sara Bals, Gino V. Baron, Pierre A. Jacobs, Bert F. Sels**

Catalyst Design by NH₄OH Treatment of USY Zeolite

